Protein Engineering, Design & Selection vol. 25 no. 10 pp. 485–505, 2012
Published online July 4, 2012 doi:10.1093/protein/gzs039

Transfer of engineered biophysical properties between different antibody formats and expression systems

Jonas V. Schaefer and Andreas Plückthun[1]

Department of Biochemistry, University of Zurich, Winterthurerstrasse 190, CH-8057 Zurich, Switzerland

[1]To whom correspondence should be addressed.
E-mail: plueckthun@bioc.uzh.ch

Received March 7, 2012; revised May 16, 2012; accepted May 21, 2012

Recombinant antibodies and their derivatives are receiving ever increasing attention for many applications. Nevertheless, they differ widely in biophysical properties, from stable monomers to metastable aggregation-prone mixtures of oligomers. Previous work from our laboratory presented the combination of structure-based analysis with family consensus alignments as being able to improve the properties of immunoglobulin variable domains. We had identified a series of mutations in the variable domains that greatly influenced both the stability and the expression level of single-chain Fv (scFv) fragments produced in the periplasm of *Escherichia coli*. We now investigated whether these effects are transferable to Fab fragments and immunoglobulin G (IgG) produced in bacteria, *Pichia pastoris*, and mammalian cells. Taken together, our data indicate that engineered mutations can increase functional expression levels only for periplasmic expression in prokaryotes. In contrast, stability against thermal and denaturant-induced unfolding is improved by the same mutations in all formats tested, including scFv, Fab and IgG, independent of the expression system. The mutations in V_H also influenced the structural homogeneity of full-length IgG, and the reducibility of the distant C_H1-C_L inter-chain disulfide bond. These results confirm the potential of structure-based protein engineering in the context of full-length IgGs and the transferability of stability improvements discovered with smaller antibody fragments.
Keywords: antibody engineering/denaturation/IgG/*Pichia pastoris*/protein stability

Introduction

Murine monoclonal antibodies first emerged as diagnostic and therapeutic agents in the late 1970s, but only the possibility to generate recombinant human and engineered antibodies by many technologies has led to their greatly accelerated adoption for human therapy. The reliable and inexpensive production of various antibody formats in recombinant form has remained one of the major objectives for antibody engineering, as antibodies differ widely in their biophysical properties. Small antibody fragments like single-chain Fv (scFv) or Fab expressed in *Escherichia coli* (Huston *et al.*, 1988; Skerra and Plückthun, 1988; Glockshuber *et al.*, 1990) have been pivotal research intermediates in essentially all antibody engineering projects, but by far most antibodies used in the clinic today have been converted to the immunoglobulin G (IgG) format (Plückthun and Moroney, 2005; An, 2010; Beck *et al.*, 2010). The main reason is that most clinical applications rely on the effector function of the IgG Fc region. Even if the expression of full-length IgG has been performed successfully in *E. coli* (Simmons *et al.*, 2002; Mazor *et al.*, 2009; Makino *et al.*, 2011), therapeutic antibodies generally are produced in mammalian cells, as only this expression system can carry out the posttranslational modifications and introduce the complex glycosylation necessary for most of the functional activities of IgG molecules.

Compared with conventional small molecules, antibody drugs offer advantages concerning their extended half-life *in vivo* and their ability for initiating host immune responses such as antibody-dependent cellular cytotoxicity (ADCC) or complement-dependent cytotoxicity (CDC) (Jefferis *et al.*, 1998). The long half-life of IgG molecules is due to the pH-dependent binding of the C_H2-C_H3 interface to the neonatal receptor FcRn, a major histocompatibility complex class I-like molecule expressed on the vascular endothelium. Binding to FcRn protects antibodies from degradation by enabling recycling of the molecules and thereby increases their serum persistence (Ghetie and Ward, 2000; Roopenian and Akilesh, 2007).

Residues located in the hinge region and the C_H2 domain contact the Fcγ receptors, and among them especially the activating FcγRIIIa is responsible for triggering ADCC by recruiting immune cells that lead to phagocytosis or lysis of the targeted cells (Jefferis *et al.*, 1998; Shields *et al.*, 2001; Lazar *et al.*, 2006; Strohl, 2009; Kaneko and Niwa, 2011). The latter interaction requires the complex glycosylation obtained from mammalian expression systems, which is not provided by yeast and plant expression systems (Jefferis, 2009; Lux and Nimmerjahn, 2011). In CDC, antibodies activate the complement cascade at the cell surface, upon being triggered by C1q binding to the C_H2 domain—eventually killing the targeted cells (Ricklin *et al.*, 2010).

IgGs are composed of various domains, all of them possessing the characteristic immunoglobulin fold consisting of two antiparallel β-sheets forming a β-sandwich (Lesk and Chothia, 1982; Padlan, 1994), which can aggregate, probably involving the β-strands, as in many aggregates of other proteins (Dobson, 2003). The overall stability of the full-length IgG molecule depends on both the intrinsic stabilities of the individual domains as well as on the stability of the corresponding interfaces (Brandts *et al.*, 1989; Wörn and Plückthun, 1998, 1999; Röthlisberger *et al.*, 2005). The various IgG domains are known to feature intrinsic differences in their conformational stability and therefore might also be responsible to different degrees for the biophysical properties of the antibody as a whole.

The IgG's antigen-binding sites are formed by the complementarity determining regions (CDRs) within the N-terminal

variable regions of both the light chain (V_L) and heavy chain (V_H) coming together and generating the unique surface that specifically recognizes and binds the corresponding antigens (Mian *et al.*, 1991). The remaining framework of the variable domains is quite conserved in both sequence and structure. Nevertheless, different families of variable domains with varying framework sequences have shown quite distinct biophysical properties (see below). The particular arrangement of the antigen-binding region within the CDRs thus permits re-engineering of the framework residues without jeopardizing antigen binding, at least to a first approximation.

Owing to the great sequence diversity within their variable regions, antibodies show a wide range of biophysical properties (Ewert *et al.*, 2003b; Garber and Demarest, 2007; Wang *et al.*, 2009). Favorable properties are important for a number of reasons (Demarest and Glaser, 2008). First, an aggregation-prone molecule would run the danger of leading to unspecific binding *in vivo*, premature clearance, loss of clinical efficacy and the danger of eliciting a T-cell-independent immune response (Maas *et al.*, 2007; Singh *et al.*, 2010). Second, the aggregation-tendency would be potentiated in fusion proteins with additional aggregation-prone domains or multimerized constructs, rendering many antibody fusions impossible to be produced efficiently. Finally, low stability and a tendency to aggregate will decrease the expression level, and may thus make otherwise promising molecules economically not viable.

In previous work (Ewert *et al.*, 2003b), we discovered surprising differences in the biophysical properties of the germline families of human V_H domains, as well as both human domains encoding the κ and λ light chain ($V_κ$ and $V_λ$), respectively. By sequence comparison of the human consensus V_H domains, particular mutations could be identified (Fig. 1a) that proved to be responsible for the favorable biophysical properties of families 1, 3 and 5, as well as for the less favorable properties of families 2, 4 and 6. Subsequently, these sequence differences were transplanted from a V_H3 consensus framework to the very poorly stable and poorly expressing V_H6 framework (Ewert *et al.*, 2003a). In brief, two non-glycine residues with positive ϕ angles in the Ramachandran plot were converted to glycines (positions 16 and 76; numbering scheme according to Honegger and Plückthun, 2001), inducing a positive effect on both thermodynamic stability and functional expression in *E. coli.* As functional periplasmic expression levels are limited by folding (Ewert *et al.*, 2003b), they constitute an excellent measure of aggregation during *in vivo* folding. In addition,

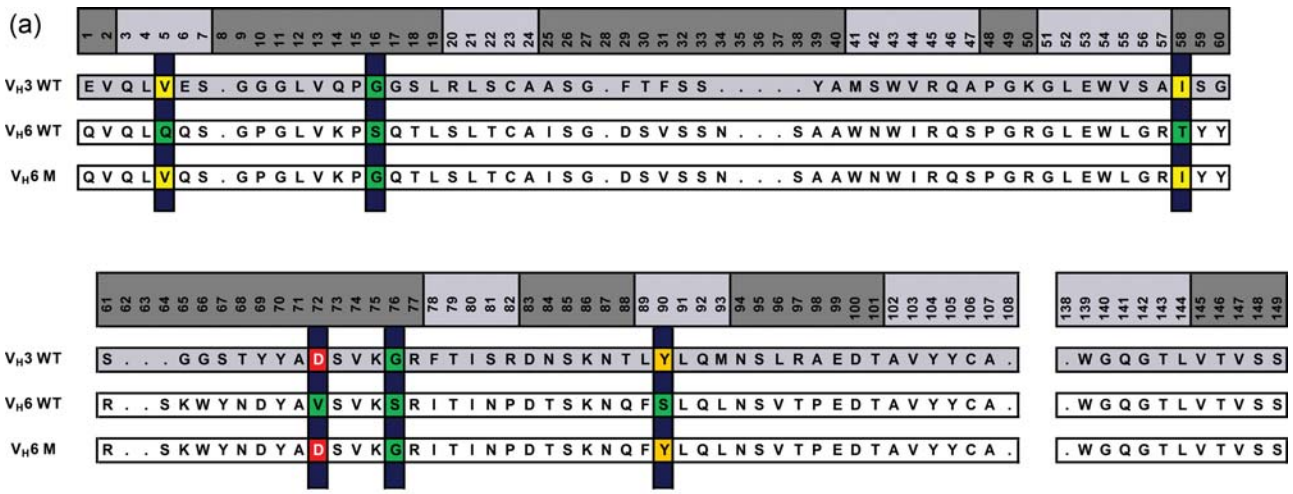

	IgG 2C2	IgG 6B3
antigen	Peptide (M18)	Protein (myoglobin)
heavy chain	V_H6	V_H6
light chain	$V_κ3$ (kappa)	$V_λ3$ (lambda)
pI (WT / M)	8.68 / 8.61	6.91 / 6.66

Fig. 1. Alignment of V_H sequences. (**a**) Comparison of HuCAL-derived WT V_H3 and V_H6 sequences (two uppermost sequences). The V_H6 domain, having aggregation-prone behavior and the lowest midpoint of denaturation, was brought closer to the V_H3 sequence as described before (Ewert *et al.*, 2003a), leading to the engineered M variant (lower line). This mutant holds the following six amino acid exchanges: Q5V, S16G, T58I, V72D, S76G and S90Y. Only mutated amino acids are highlighted and color-coded according to residue type: aromatic (orange), hydrophobic (yellow), uncharged hydrophilic residues (green) and acidic (red). The numbering scheme is according to Honegger and Plückthun (2001). (**b**) Summary of the two different IgG constructs, 2C2 and 6B3, analyzed in this study. (**c**) SDS-PAGE analysis of equal amounts of the Protein A-purified IgG constructs under reducing conditions, stained with Coomassie Blue.

two residues with non-optimal β-strand forming features were exchanged to amino acids possessing higher β-sheet propensity (Q5V and S90Y), both affecting functional expression, but only the first having a significant thermodynamic equilibrium effect. The removal of a buried non-hydrogen-bonded OH group (T58I) led to a very large increase in thermodynamic stability, but no effect on folding yield. Conversely, the mutation of a solvent-exposed hydrophobic residue to a hydrophilic one (V72D) increased the *in vivo* folding yield but had very little effect on thermodynamic stability.

All the selected mutations (Q5V, S16G, T58I, V72D, S76G and S90Y) were located within the V_H framework and not in the CDRs, as these mutations were intended to be as generally applicable as possible and unlikely to affect antigen binding. As intended, the combined mutations conferred properties almost identical to the favorable V_H3 framework on the V_H6 framework (Ewert *et al.*, 2003a), which afterwards experienced a dramatic increase in both expression yield and thermodynamic stability without having altered binding properties.

These data were recorded for two model antibody scFvs named 2C2 and 6B3 that had originally been selected from the HuCAL library (Knappik *et al.*, 2000) by panning against the peptide M18 coupled to transferrin or myoglobin from horse skeletal muscle, respectively. We chose these molecules as both are representatives of the human V_H6 framework family whose members are known to have a rather aggregation-prone behavior and the lowest thermodynamic stability of all human V_H domains (Ewert *et al.*, 2003b). 2C2 and 6B3 have different CDR-H3 loops, while otherwise their V_H sequence is identical. In addition, the two antibodies (compared in Fig. 1b) differ in their respective light chain, with 2C2 having a $V_κ3$ and 6B3 containing a $V_λ3$ light chain. Importantly, the previously detected improvements were independent of both the V_L domain as well as the sequence and length of the CDR-H3, as both constructs gave similar results (Ewert *et al.*, 2003a).

These improvements had been uncovered and investigated with antibody constructs small enough to untangle the contributions of the individual domains with spectroscopic investigations, using scFv constructs which consist of just two domains. However, the question arose, whether the rather dramatic effects of these mutations might somehow be dampened in a larger assembly, such as a whole IgG, and whether the eukaryotic secretory quality control (Anelli and Sitia, 2008) might overcome all folding issues seen in *E. coli.* Thus, we now tested the influence of these well-characterized mutations in the context of full-length human IgG1 or Fab molecules expressed in eukaryotic systems. Both the wild-type (WT) and best engineered variant (carrying all six mutations described above, called 'M' for 'mutant' in this study) were converted to the Fab or full-length IgG format and investigated for their biophysical properties and expression characteristics upon production in human embryonic kidney (HEK) 293 cells and the yeast *Pichia pastoris* (PP). After Protein A purification, these molecules show the expected running behavior in reducing sodium dodecyl sulfate polyacrylamide gel electrophoresis (SDS PAGE) (Fig. 1c).

To be able to carry out such studies with whole IgGs or Fab fragments, eukaryotic expression systems were required where functional expression yields would exclusively depend on the protein sequence. Therefore, these systems must rely both on homologous recombination to exactly the same locus and on constitutive expression to eliminate complication from the induction strategy. For Fab and IgG production in HEK293 cells, stable cell lines were created using the Flp-In system (Invitrogen). These cell lines expressed and secreted the antibody constructs under control of the constitutive cytomegalovirus (CMV) promoter in sufficient amounts, allowing the purification and subsequent biophysical analysis of these proteins. As *Pichia* does not maintain episomal vectors, expression cassettes were anyway designed for integration into the yeast genome. To ensure a comparable expression setup between mutants, the constitutive GAP promoter was used.

In this study, we compare the effects of the previously described mutations on the biophysical properties of antibodies in the IgG and Fab format, produced in mammalian and yeast cells, using a wide array of biophysical techniques. We also analyze the effect of the mutations on the expression levels in bacteria, yeast and mammalian cells—allowing a differentiation of how the various cellular hosts deal with aggregation-prone proteins in general.

Materials and methods

Cell culture

Materials and cultivation of mammalian and Pichia cells. All media and supplements for mammalian expression were purchased either from Sigma-Aldrich (MO, USA), Invitrogen (CA, USA) or Amimed (BioConcept, Switzerland). The antibiotics Zeocin™ and Hygromycin B were bought from Invitrogen or PAA (Austria), respectively. All solutions used were either delivered sterile or sterilized by filtration through 0.22 μm filters (Millipore, MA, USA). Stably transformed HEK293 cells were maintained in Dulbecco's modified Eagle medium (DMEM; Sigma-Aldrich; high glucose: 4.5 g/l) supplemented with 10% v/v heat-inactivated fetal bovine serum (FBS; Amimed) in a humidified incubator with 5% carbon dioxide at 37°C. Expression of IgGs was carried out in DMEM supplemented with 5% v/v FBS (instead of the more commonly used 10%). For secretion of IgGs, derivatives of the vector pcDNA5 (Invitrogen) containing constitutively active CMV promoters upstream of the native IgG signal sequences were used (see below).

For all work with *Pichia*, the strain SMD1163 (*his4 pep4 prb1*; Invitrogen) was used. All media and supplements for this work were purchased either from Sigma-Aldrich or Invitrogen. All work was done in a sterile laminar flow bench, and yeast growth was performed at 30°C. Selection of clones stably expressing the IgGs was based on Zeocin™ resistance. For secretion of IgGs, derivatives of the pGAPZαB vector (Invitrogen) containing the constitutively active *Pichia* GAP promoter followed by the α-factor pre-pro (αMFpp) region were used. Yeast extract-peptone-dextrose (YPD) medium containing 20 g/l peptone, 10 g/l yeast extract and 20 g/l D-glucose (plus 20 g/l agar for YPD-agar) was used for routine growth and subculturing of *Pichia* cells. Zeocin™ was added to a final concentration of 100 μg/ml. IgG expression was performed in the phosphate-buffered medium with glycerol for yeast (BMGY) (20 g/l peptone, 10 g/l yeast extract, 100 mM potassium phosphate pH 6.0,

1.34% yeast nitrogen base (YNB) without amino acids, 1% w/v glycerol, 400 μg/l biotin) in the absence of antibiotic.

Construction of expression plasmids. Unless stated otherwise, all molecular biology methods were performed according to standard protocols (Sambrook and Russell, 2001). All enzymes used for cloning were purchased from New England Biolabs (MA, USA) or Fermentas (Germany). In general, cloning and propagation of all plasmids was carried out in *E. coli* DH5α (Life Technologies, CA, USA), grown at 37°C in low salt LB Broth (10 g/l Bacto-tryptone, 5 g/l yeast extract, 5 g/l NaCl, pH 7.5) containing 25 μg/ml Zeocin™ for the *Pichia* plasmids or in 2YT broth (16 g/l Bacto-tryptone, 10 g/l yeast extract, 5 g/l NaCl, pH 7.5) containing 100 μg/ml Ampicillin (AppliChem, Germany) for mammalian vectors.

The construction of expression vectors is described in detail in the Supplementary Material. In brief, expression vectors for mammalian HEK293 cells were derived from the pMORPH® vector series (MorphoSys), in which heavy or light chain are separately expressed. For the establishment of stable cell lines using the Flp-In system (Invitrogen), the two expression cassettes for H and L, each retaining its own promoter and poly-A sequence, were combined into a single vector based on the pcDNA5/FRT series (Invitrogen). The creation of Fab expression vectors was performed likewise, in this case, however, the V_H/C_H1 chain was fused to a myc-tag and $(his)_6$-tag at its C-terminus for detection and purification purposes.

The *Pichia* expression vectors are based on the vector pGAPZαB (Invitrogen). The sequences for the light chains and the different heavy-chain variants were amplified from the pMORPH® vectors and thus placed behind the α-factor pre−pro (αMFpp) sequence and under the control of the constitutive GAP promoter. Before stable integration into the *Pichia* genome, the two expression cassettes for H and L, each retaining its own promoter and termination sequence, were combined onto one plasmid.

Construction of glycan knock-out mutants T299A. To analyze the influence of the glycan moiety attached to Asn297 in the C_H2 domain of the heavy chains, the glycan knock-out construct T299A was constructed, described in detail elsewhere (Schaefer and Plückthun, 2012). In brief, ACG coding for the threonine in the glycosylation motif Asn_{297}-Ser_{298}-Thr_{299}, was mutated to alanine-encoding GCG using the QuikChange® site-directed mutagenesis kit from Stratagene (acquired by Agilent, USA) according to the manufacturer's instructions.

Creation of stable cell lines. Flp-In HEK293 cell lines (Invitrogen), stably expressing the IgG of interest and secreting it into the culture medium, were generated according to the instructions of the Flp-In system manual. For this purpose, the expression cassettes for both the heavy- and light-chain genes were cloned into the pcDNA5/FRT vector and finally inserted at a specific location in the genome by the Flp recombinase within the cell. After selection, 10 single clones of each construct were tested for expression of the desired IgG by western blot analysis of the supernatant. More than 90% of the analyzed clones were positive.

For the *Pichia* constructs, the corresponding plasmids containing both genes for the light and heavy chain under the control of constitutively active GAP promoters within one plasmid were linearized by *Bgl*II and integrated into the yeast genome upon transformation of competent *Pichia* (Cregg *et al.*, 2009). Finally, several colonies per construct were re-plated on fresh YPD-agar plates containing Zeocin™ and subsequently analyzed for IgG expression by western blot.

Expression of IgG. Large-scale expression in the mammalian and the yeast system is described in detail elsewhere (Schaefer and Plückthun, 2012). Prokaryotic expression of IgG was performed in *E. coli* SB536 (WG1 *ΔfhuA ΔhhoAB* (Bass *et al.*, 1996)) in small scale. Both chains were placed in a bicistronic ORF within pMORPH®X7 derivatives (MorphoSys; (Cesaro-Tadic *et al.*, 2003)) under an inducible lac promoter/operator. Pre-cultures of 5 ml 2YT medium containing 1% glucose were inoculated with a single colony and incubated at 37°C overnight. The expression cultures (10 ml 2YT with 0.1% glucose) were inoculated with the pre-cultures at an OD_{600} of 0.1 and grown at 30°C for 20 h. IgG synthesis was not actively induced by adding inducer but rather driven from the leaky expression once all glucose was consumed. IPTG addition only marginally increased the amount of full-length IgG but lead to more partially assembled molecules (like HL and H_2L intermediates). The next day, the cultures were OD-normalized and molecules in the periplasmic space were extracted by incubation of the cell pellet for 2 h at 4°C in the presence of 200 mM boric acid, 160 mM NaCl, 2 mM ethylenediaminetetraacetic acid (EDTA), pH 8.0. Finally, the expression levels of WT and M variants were compared by western blots using anti-light chain-specific antibodies as described below.

Biophysical and biochemical analysis

Purification of IgGs. Antibodies were purified from culture supernatants by Protein A affinity chromatography. For this purpose, the supernatants were loaded onto HiTrap Protein A columns (GE Healthcare, USA) at 4°C at a flow rate of 1 ml/min. Chromatography was performed using an ÄKTA PrimePlus chromatography system (GE Healthcare) at 4°C. After loading, the column was washed with 100 mM sodium phosphate buffer pH 8.0 containing 150 mM NaCl. Elution of IgG was accomplished by using 0.1 M glycine pH 2.7, followed by immediate neutralization of each fraction to pH 7.5 using 1 M Tris, pH 8.0. The concentrations of the sample fractions were determined by UV-spectroscopy at 280 nm with a NanoDrop ND-1000 spectrophotometer (Thermo Scientific), assuming a mass extinction coefficient of 1.37 for a 1 mg/ml solution of IgG. The samples with the highest protein concentration were pooled and dialyzed twice against phosphate buffered saline (PBS; Sigma-Aldrich; 10 mM Na_2HPO_4, 1.8 mM KH_2PO_4, 2.7 mM KCl, 137 mM NaCl, pH 7.1) at 4°C. After dialysis, the samples were filtered through 0.22-μm filters (Millipore) and stored at 4°C.

Sodium dodecyl sulfate-polyacrylamide gel electrophoresis and western blotting. Sodium dodecyl sulfate-polyacrylamide gel electrophoresis (SDS-PAGE) was performed using either NuPAGE precasted 4–12% gradient gels (Invitrogen) according the manufacturer's instructions or

self-made Tris-glycine 7.5% or 12% gels for non-reduced or reduced samples, respectively. Gels and samples were prepared according to standard protocols (Laemmli, 1970) and 1.5 μg of IgG antibody was loaded per lane. Non-reduced samples were only mixed with loading buffer, while for reduced samples dithiothreitol (DTT) was added to a final concentration of 16 mM, followed by incubation for 5 min at 95°C. As molecular mass marker the PageRuler prestained protein ladder (Fermentas) was used. The gels were stained using Coomassie following standard protocols or by silver staining according to the manufacturer's instructions (Invitrogen).

For the specific detection of the IgGs, the proteins were transferred to a polyvinylidene difluoride membrane (Millipore) after their separation by SDS-PAGE. Blotting was performed following the semi-dry method within a Trans-Blot SD cell (Bio-Rad, CA, USA) for 60 min at 11 V, using a Tris–glycine buffer (20 mM Tris, 150 mM glycine, 10% methanol). After blocking the membrane in 5% MPBST (5% w/v skimmed milk dissolved in PBST (PBS with 0.05% Tween-20)) for at least 1 h, the membrane was incubated for another hour in 2.5% MPBST containing the appropriate detection antibody conjugated to alkaline phosphatase. For detection of the light chains, an anti-human lambda-light chain-specific antibody (Sigma-Aldrich, #A2904; 1 : 1500 dilution) or an anti-human κ-light chain-specific antibody (Southern Biotech, #2060-04; 1 : 3000 dilution) were used. Bands were detected by the addition of NBT-BCIP solution (nitro-blue tetrazolium chloride with 5-bromo-4-chloro-3′-indolyphosphate p-toluidine salt; Sigma-Aldrich) in 100 mM Tris pH 9.5, 5 mM $MgCl_2$, 100 mM NaCl. The development was terminated when the first bands became clearly visible by rinsing the membrane in ultra high pure water.

Isoelectric focusing. Determination of the isoelectric point (pI) of the constructs was carried out in isoelectric focusing (IEF) Ready Gels (pH 5–8; Bio-Rad) according to the manufacturer's instructions on a Mini-PROTEAN II vertical cell system (Bio-Rad), using increasing voltages (100 V for 1 h, 250 V for 1 h, and 500 V for 30 min). Next to the samples, an IEF standard (Bio-Rad) was co-electrophoresed. The cathode and anode buffers were 20 mM lysine/20 mM arginine or 7 mM phosphoric acid, respectively. Following electrophoresis, the proteins were visualized by Coomassie Blue—Crocein Scarlet staining (0.04% w:v Coomassie R-250 and 0.05% w:v Crocein Scarlet 3B in 27% isopropanol/10% acetic acid) for 45 min and destaining (40% methanol/10% acetic acid).

Capillary electrophoresis. Capillary electrophoresis was performed on the chip-based Lab-Chip 90 instrument (Caliper Life Sciences, MA, USA) under non-reducing and reducing conditions following the manufacturer's instructions with slight modifications. In brief, 5 μl sample containing 2.5 μg IgG was mixed with 35 μl of denaturation solution and incubated either at 25°C or 75°C for 5 min. The denaturation solution was prepared according to the provided protocol either without any reducing agent or by the addition of DTT in the recommended concentration. Seventy microliters of distilled water were added to each sample prior to analysis and the analysis chip was primed according to the manufacturer's instructions. The automated protein analysis generated both a chromatogram (showing migration time) as well as a virtual gel (mimicking a Coomassie-stained gel) as output.

2D-electrophoresis with SDS-PAGE in both dimensions. To analyze whether the different banding patterns in WT and M samples consist of species which can be separated or species which re-equilibrate, a 2D-SDS-PAGE was devised. Gels were run in a cold room. Duplicates of 4 μg IgG samples were run for the first dimension on an SDS-PAGE gel on two identical halves. While one half of the gel (containing one of the duplicates each) was used for Coomassie staining of the protein bands, the second half was stored temporarily in SDS-running buffer. After the bands were clearly visible, either the corresponding positions or whole lanes on the unstained gel half were cut and placed on top of the second SDS polyacrylamide gel in perpendicular orientation. This resulted in the re-separation based on the size of the proteins in the second dimension as well. To prevent air bubbles to influence the running behavior, the placed pieces of gel were mounted with regular stacking gel material poured round the gel pieces. The final gel was stained using the Silver Quest kit (Invitrogen) according to the manufacturer's instructions.

Analysis of IgG and Fab expression levels by enzyme-linked immunosorbent assay. To analyze the influence of the performed mutations on the antibody expression and secretion levels, the same number of HEK293 cells stably expressing the corresponding IgG or Fab constructs was seeded in 12-well plates. On reaching confluency, the medium was removed and replaced by 1 ml expression medium, containing 5% FBS. Twenty-four hours later, the supernatant was analyzed for its IgG or Fab content by enzyme-linked immunosorbent assay (ELISA). For the *Pichia*-produced IgGs, OD-normalized aliquots were taken after 24 h expression for ELISA analysis. For the IgG detection ELISA, a capture antibody recognizing the human IgG heavy chain (Jackson ImmunoResearch, PA, USA; #209-005-098) was immobilized on MaxiSorb plates (Nunc) overnight at 4°C. For detection of Fab fragments in the supernatant, an anti-myc capture antibody (Sigma-Aldrich, #M4439; 1 : 2000 dilution) was coated on the plates. After 1 h blocking in 5% skimmed milk in PBST, 100 μl of *Pichia* or HEK-derived supernatant (diluted in a range of 1 : 25 to 1 : 100 in fresh BMGY or DMEM media) was incubated for 1 h at room temperature. The expressed IgG or Fab molecules were detected by incubating with an anti-human lambda-light chain-specific antibody conjugated to alkaline phosphatase (Sigma-Aldrich, #A2904; 1 : 2000 dilution) for 1 h and subsequent addition of *p*-nitrophenyl phosphate (Sigma-Aldrich). Absorbance at 405 nm was measured using a Perkin Elmer HTS 7000 Plus plate reader by sampling up to 1 h.

To analyze the levels of IgG still present within the cells, cells stably expressing the IgG constructs were cultured in 12-well plates for 3 days in duplicates. The supernatant was harvested, the cells washed twice with PBS and finally 250 μl of radioimmunoprecipitation assay buffer (50 mM Tris pH 7.5, 150 mM NaCl, 1% NP40 and 0.25% Na-deoxycholate) added to the cells before the plates were placed at −80°C for 2 h. After this freezing-thawing step, the cells were scraped off and the extracts were subsequently analyzed by SDS-PAGE followed by Coomassie staining or by western blotting. To allow the simultaneous detection of

IgG in the supernatant and the cellular extracts on the same gel, only 1/6 of the corresponding supernatant was loaded compared with the cellular extract, and all samples were heated to 95°C for 5 min prior to loading.

Circular dichroism spectroscopy. Circular dichroism (CD) measurements were performed on a Jasco J-810 Spectropolarimeter (Jasco, Japan) equipped with a computer-controlled water bath (refrigerated circulator FS18, Julabo, Germany), using a 0.5-mm cylindrical thermocuvette. CD spectra were recorded from 200 to 250 nm with a data pitch of 0.5 nm, a scan speed of 20 nm/min, a response time of 4 s, and a bandwidth of 2 nm. Measurements were performed at 25°C and each spectrum was recorded three times and averaged. The CD signal was corrected by buffer subtraction and converted to mean residue ellipticity (MRE) using the concentration of the sample determined spectrophotometrically at 280 nm. Heat denaturation curves were obtained by measuring the CD signal at 208 nm at temperatures increasing from 25°C to 90°C (heating rate 1°C/min; response time 4 s; bandwidth 2 nm). Data were collected and processed as described above. CD spectra and denaturation curves of the purified IgGs were measured in PBS (Sigma-Aldrich; pH 7.1) at a protein concentration of 5 μM.

Intrinsic tryptophan fluorescence. Intrinsic tryptophan fluorescence (ITF) was measured with a Jobin-Yvon Fluoromax-4 spectrofluorimeter (Horiba Scientific, NJ, USA) equipped with a Peltier-controlled cuvette holder. The temperature was controlled by an LFI3751 5A digital temperature control instrument (Wavelength Electronics Inc., MT, USA). Upon excitation at 295 nm, Trp emission spectra were recorded from 300 to 400 nm ($\Delta\lambda = 1$ nm, scan rate 1 nm/s) in 0.5°C steps from 25°C to 90°C. The sample cuvette was equilibrated for 2 min at each temperature to ensure that the desired temperature was reached within the cell. Protein concentrations were 1 μM in every case, and all measurements were performed in PBS (pH 7.1). The intensity of the emission spectrum at 330 nm (F_{330}) and 350 nm (F_{350}) was determined at each temperature, the ratio F_{330}/F_{350} calculated and subsequently plotted as a function of temperature.

For the analysis of the midpoints of denaturation at various pH, IgGs were dialyzed overnight and analyzed at the conditions described above in the following buffers. For pH 4 and 5: 25 mM sodium acetate, 130 mM NaCl; for pH 6, 7 and 8: 25 mM sodium phosphate, 130 mM NaCl; for pH 9 and 10: 25 mM sodium carbonate, 130 mM NaCl.

Guanidine hydrochloride-induced equilibrium unfolding. Guanidine hydrochloride (GdnHCl)-induced denaturation measurements were carried out with protein/GdnHCl mixtures containing a final protein concentration of 1 μM and denaturant concentrations ranging from 0 to 5 M (99.5% purity; Fluka, MO, USA). These mixtures were prepared from a 6 M GdnHCl stock solution (in PBS, pH adjusted to 7.1) and equilibrated overnight at 25°C. Each final concentration of GdnHCl was determined by measuring the refractive index. The intrinsic fluorescence emission spectra were then recorded from 300 to 400 nm with an excitation wavelength of 295 nm in an Infinite M1000 reader (Tecan, NC, USA). Individual GdnHCl blanks were recorded and automatically subtracted from the data. The emission ratio F_{330}/F_{350} was calculated and plotted as a function of GdnHCl concentration. Time-dependent unfolding was recorded with the same setup in a Jobin-Yvon Fluoromax-4 spectrofluorimeter (Horiba Scientific, NJ, USA), recording full spectra every 2 min for 5.5 h, starting at the time of GdnHCl addition without any previous incubation.

Size-exclusion chromatography. Size-exclusion chromatography (SEC) experiments were performed using a Superdex 200 PC 3.2/30 column (GE Healthcare). The runs were performed in PBS buffer (Sigma-Aldrich, pH 7.1) at a flow rate of 0.06 ml/min at 25°C on an ÄKTA Micro system (GE Healthcare). Samples of 50 μl containing 6.7 μM IgG were injected and protein elution was monitored at 280 nm. Cytochrome c (12.4 kDa), albumin (66 kDa) and β-amylase (200 kDa) were used as standards to calibrate the column.

Reverse phase-high-performance liquid chromatography analysis. High-performance liquid chromatography (HPLC) analyses were performed according to Dillon *et al.* (2006) on an Agilent 1100 HPLC system equipped with a binary pump. Samples were separated on a Zorbax SB300 C8, 3.5 μm at 75°C with a flow rate of 0.25 ml/min. The following setup was used for all runs: solvent A: 0.1% TFA, solvent B: 0.09% TFA/9.9% water/20% acetonitrile/70% isopropanol. The column was initially equilibrated with 90% mobile phase A and 10% mobile phase B for 5 min followed by a 2-min step gradient from 10 to 25% B. Elution was achieved with a linear gradient of 25–40% B over 18 min. Afterwards a final flush of 90% B was performed for 5 min and the system set back to initial conditions and equilibration for 11 min prior to the next run (total run time = 45 min). Reduced samples were adjusted to 4.2 M GdnHCl/70 mM Tris/3.5 mM EDTA, pH 8.6 in the presence of 50 mM DTT and incubated at room temperature for 2 h prior to analysis.

Cation-exchange chromatography. Cation-exchange chromatography (CIEX) was carried out on an Agilent 1100 binary pump LC system equipped with a TSKgel CM-STAT column, 7 μm, 4.6 × 100 mm column (Tosoh Bioscience, Japan). Thirty micrograms of purified IgGs were injected onto the column equilibrated in buffer A (25 mM sodium phosphate pH 6.0). Antibodies were eluted by a linear gradient to 30% buffer B (25 mM sodium phosphate pH 6.0, 1 M sodium chloride) over a 30-min time period with detection at 280 nm. The column temperature and flow rate were maintained at 25°C and 0.5 ml/min, respectively.

Differential scanning calorimetry. Differential scanning calorimetry (DSC) measurements were performed using a VP-Capillary DSC system (Microcal Inc., acquired by GE Healthcare). The antibody concentrations were adjusted to 0.5 mg/ml prior to the measurement. The corresponding buffer was used as a reference. The samples were heated from 15°C to 100°C at a rate of 1°C/min after initial 8 min of equilibration at 15°C. A filtering period of 10 s was used and data were analyzed using Origin 7.0 software (OriginLab Corporation, MA, USA). Thermograms were corrected by subtraction of buffer-only scans and then normalized to the molar concentration of the protein. The final excess heat-capacity thermogram was obtained by interpolating a cubic baseline in the transition region. The midpoint of a thermal

transition temperature (T_m) was obtained by analyzing the data using Origin 7 software provided with the instrument. As all measured transitions are irreversible, all the experimental values reported in this study for melting temperatures have to be regarded as 'apparent' values.

Differential-scanning fluorimetry. Differential scanning fluorimetry (DSF) was performed using the Rotor-Gene Q real-time PCR cycler (QIAGEN) and fluorescence data were collected using the instrument's HRM channel settings (λ_{ex} 460 nm; λ_{em} 510 nm). The SYPRO Orange dye (Molecular Probes; see Volkova *et al.* (2007) for a partial structure) in dimethyl sulfoxide was diluted 500-fold from the supplied stock solution into the appropriate buffers just prior to being added to the protein solutions. The samples with a final protein concentration of 3.5 μM in 20 μl reaction mixture were subjected to a temperature ramp from 30°C to 90°C at a heating rate of 1°C/min and at 0.5°C increments with an equilibration time of 30 s at each temperature prior to measurement. The T_m was determined as the temperature corresponding to the maximum value of the first derivative of the fluorescence changes, calculated by the software. When multiple unfolding transitions were observed, only the T_m value of the first transition could be accurately determined, as the transitions at higher temperatures overlap. Prior to the DSF analysis, several IgGs were analyzed by fluorescence spectroscopy in the presence or absence of SYPRO Orange. In agreement with the literature, the dye did not induce any changes in the thermal stability determined by ITF, as long as the final dye concentration was lower than a 1 : 200 to 1 : 500-fold dilution of the original reagent.

Microscale thermophoresis measurements. Binding affinities of purified IgGs to their antigen myoglobin (Sigma-Aldrich) or M18-Transferin (Jerini GmbH, Germany), respectively, were measured using microscale thermophoresis (NanoTemper, Germany) as described previously (Wienken *et al.*, 2010). Myoglobin or M18-Transferin was fluorescently labeled according to the manufacturer's instructions with a reactive NT-647 dye using N-hydroxysuccinimide ester-chemistry which reacts with primary amines to form dye–protein conjugates. For each analyzed construct, a titration series with constant antigen concentration (20 μM) and varying IgG concentrations between 10^{-11} and 10^{-5} M was prepared in PBS. The mixed samples were equilibrated for 1 h at room temperature and ~4 μl of each sample was loaded in the capillary. An infrared laser diode within the Monolith NT.115 instrument (NanoTemper, Germany) was used to increase the temperature by 4 K in the beam center. Throughout the measurement, the fluorescence inside the capillary was recorded by a CCD camera and the normalized fluorescence was plotted afterwards against the IgG concentrations. The K_D values were subsequently obtained from fitting the binding curves using Prism 5 (GraphPad, CA, USA).

Partial reduction. Partial reduction of IgGs was performed by incubating the samples in 30 mM tris(2-carboxyethyl) phosphine (TCEP) for 10 min at 25°C. Afterwards, the samples were analyzed without further heating by non-reducing SDS-PAGE and either stained by Coomassie or analyzed by western blot.

Fluorescent labeling of free sulfhydryls with 5-iodoacetamidofluorescein (5-IAF; Thermo Fischer) was performed after incubation of IgG with low μM concentrations of TCEP (corresponding to 2–10 molar equivalents; higher concentrations interfered with the subsequent 5-IAF coupling) for 1 h at room temperature. Afterwards the partially reduced samples were incubated with 5-fold molar excess of 5-IAF for 2 h at room temperature protected from light. Afterwards the samples were separated by non-reducing or reducing SDS-PAGE and the fluorescently labeled bands detected using the LAS3000 chemiluminescence detection system (Fuji, Japan). Finally, all protein bands were visualized by Coomassie staining.

Results

Expression levels of engineered Fab and IgG formats

We first analyzed the secretion levels of correctly assembled antibodies in the Fab and IgG format by ELISA (depicted in Fig. 2). To compare the improvements caused by the mutations, the expression yields are normalized relative to the yield of the corresponding WT variants. Whereas for the scFv fragments produced in *E. coli* the engineered M variant previously showed an increase in yield of 4.2- or 4.3-fold respectively, (Ewert *et al.*, 2003a), (Fig. 2a), the variable domain mutations only had a slight influence on the expression level of antibodies in eukaryotic expression systems. Whereas for the *Pichia* system (Fig. 2d), the M variants still were secreted at 15–40% increased levels, no difference could be detected for the expression of either Fab fragments or full-length IgGs in the HEK system (Fig. 2b and c).

To ensure that these results were not distorted by molecules still trapped within the cell due to an overload of the secretory pathway, the secreted IgG amounts were compared with the intracellular levels (Supplementary Data Fig. S1a). Considering that the secreted samples of each construct loaded onto the blot were diluted 1 : 6 compared with the corresponding intracellular fractions, the blot unambiguously indicated that the majority of molecules were secreted for both IgG variants. Similar results were obtained when analyzing the intracellular and extracellular IgG levels in the *Pichia* system (data not shown). Interestingly, the analysis of IgG levels secreted to the periplasm of *E. coli* had quite a different outcome (Supplementary Data Fig. S1b): the comparison by western blot clearly showed increased expression levels for the M variants even in the IgG format produced in the prokaryotic system.

Analysis of biophysical properties of full-length IgG molecules

For an analysis of their biophysical properties, IgGs were expressed either in the HEK or *Pichia* system in large scale and purified by Protein A affinity chromatography. The samples were of high purity and gave rise to the two expected bands under reducing conditions (see Fig. 1c; the heavy chain was detected at ~50 kDa and the respective light chains in the range of 23–27 kDa). As depicted in Supplementary Data Fig. S2 in extracts for the HEK produced IgGs, the purified WT and M molecules behaved as monomers in SEC but showed different elution profiles in reverse phase HPLC (RP-HPLC) and cation CIEX. These differences, however, could be accounted for by the

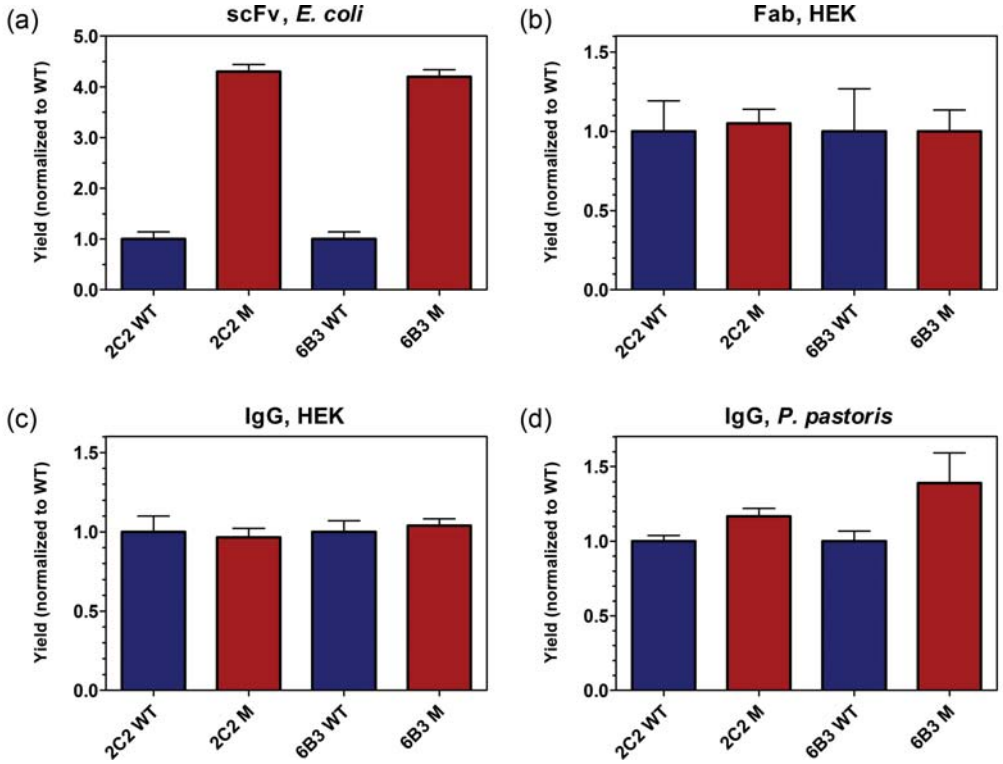

Fig. 2. Influence of mutations on secretion levels of antibody constructs. Secreted antibody levels of either scFv, Fab or IgG constructs detected by ELISA. For a better comparison, the secretion yield of soluble protein is normalized relative to the yield of the corresponding WT construct. The WT constructs are displayed in blue and the M variants in red. (**a**) Levels of scFv fragments found in the periplasm of *E. coli* (Ewert *et al.*, 2003a). (**b**) Amounts of Fab fragments secreted by stable HEK clones. (**c**) IgG levels found in the supernatant of stable HEK clones. (**d**) IgG amounts detected in the supernatant of stable *Pichia* clones.

introduced mutations themselves, influencing both the hydrophobicity as well as the charge of the engineered M variants. The net hydrophobicity of the engineered M variants was slightly increased by the two mutations Q5V and T58I, while only being lowered by a single mutation (V72D). The analysis of reduced samples by RP-HPLC (depicted in the lower halves of Supplementary Data Fig. S2c and S2d) clearly indicated that the difference in the running behavior was caused by the mutated heavy chains, as the corresponding light chains—eluting earlier than the heavy chains due to their lower hydrophobicity—led to identical signals for both variants. The additional negative charge through the V72D mutation influenced the CIEX running behavior of the engineered IgG, causing the M variants to elute at higher volumes (Supplementary Data Fig. S2e and S2f).

In addition, the binding affinity of the IgG molecules toward their corresponding antigens was confirmed to be fully retained (Supplementary Data Fig. S3). From microscale thermophoresis measurements (Wienken *et al.*, 2010), the K_D for the HEK IgG 2C2 was calculated to be 217 ± 54 and 270 ± 76 nM for the WT and M variants, respectively, while the analogous variants for the 6B3 constructs showed affinities of 15.7 ± 4.8 and 14.5 ± 3.8 nM, respectively. The slight differences of these K_D values are all within the experimental error range.

To confirm that the mutations did not influence the overall structure of the new antibody molecules, HEK and *Pichia* produced IgGs were analyzed by CD. As shown in Fig. 3a and b, the new M constructs possessed as expected the β-sheet structure typical for IgG molecules with only slight alterations. As the signals stemming from the IgG's β-sheets and random coil essentially canceled out to zero at 208 nm, thermal denaturation of the IgG molecules was determined at this wavelength as a function of temperature (Fig. 3c–f). The abrupt upward jumps seen between 75°C and 90°C in most of the depicted CD vs. temperature curves were caused by the formation of insoluble aggregates in the respective samples. Interestingly, the used expression system (HEK vs. *Pichia*) not only caused a slightly different temperature of unfolding onset, but, unexpectedly, also resulted in very different aggregation susceptibilities of the IgGs—with the 6B3 variants expressed in *Pichia* not exhibiting any detectable aggregation at all (Fig. 3f). These effects, caused by differences in the N-linked glycosylation and by an incomplete processing of the α-factor pre–pro sequence at the yeast constructs, have been studied extensively and reported elsewhere (Schaefer and Plückthun, 2012). For this study, however, we concentrated on the comparison of WT and M variants. For the 2C2 construct, no significant difference in stability between WT and M could be detected for IgGs produced in either expression system. The different signal level in Fig. 3c for the M variant was caused by its slightly off-set curve as also depicted in Fig. 3a. We currently do not know what causes this offset. For the 6B3 M construct, however, increased stabilities of ∼2.5°C were seen compared with 6B3 WT expressed in either the HEK or the *Pichia* system, as shown in Fig. 3d and f.

As the method of analyzing thermal stabilities by CD averages all changes observed over the whole IgG molecule and thus does not allow to attribute them to particular

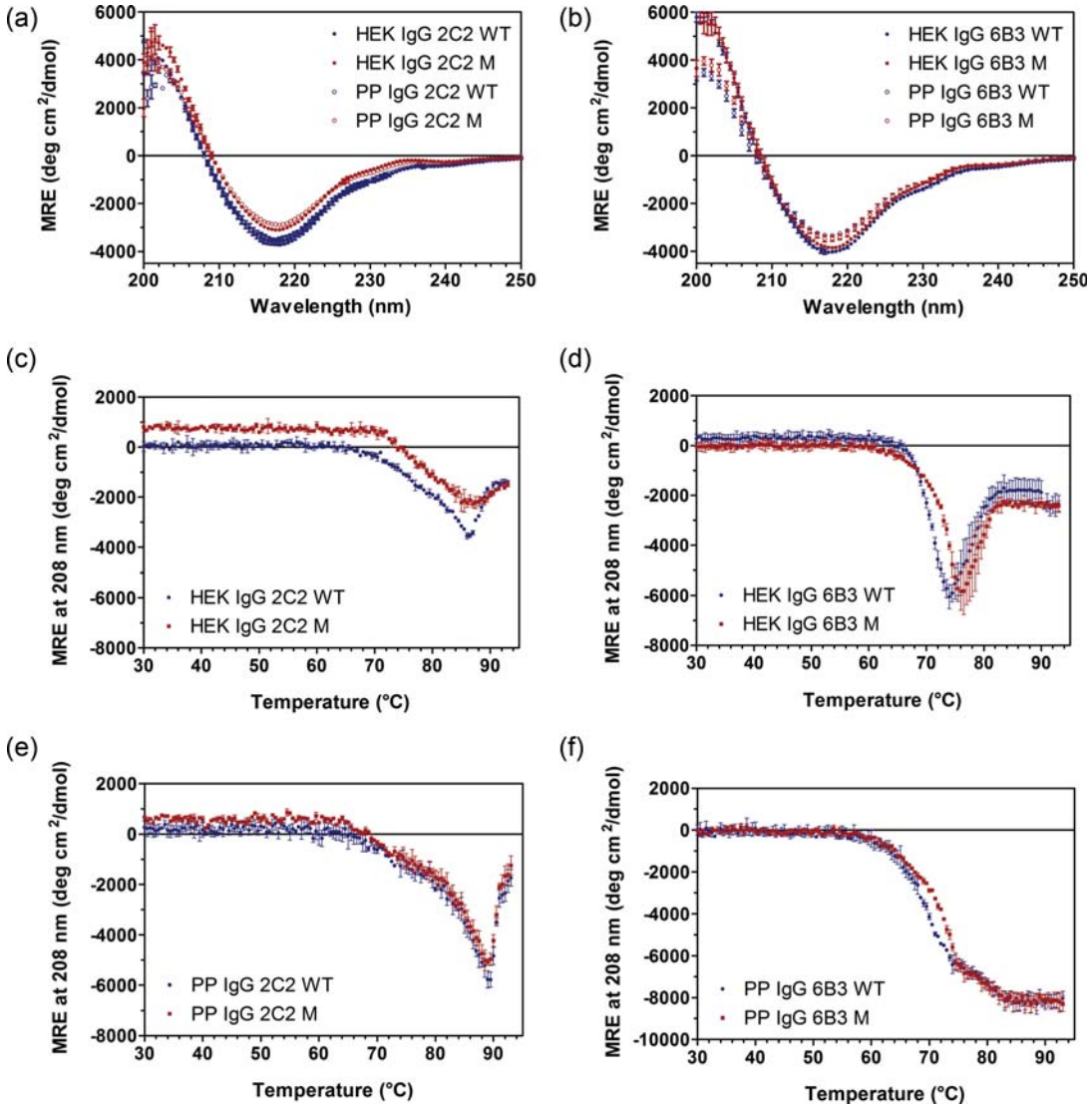

Fig. 3. Analysis of IgG constructs by CD. Signals derived from WT variants are displayed in blue while those of the mutant M are represented in red. (**a**) CD spectra of different IgG 2C2 variants produced in mammalian cells (HEK) or in the yeast *Pichia pastoris* (PP), respectively. The values are reported as mean residue ellipticity (MRE). (**b**) CD spectra of different IgG 6B3 variants analogous to panel (a). (**c**) Thermal denaturation curves of IgG 2C2 produced in mammalian cells. The denaturation was followed by CD, plotting the signals at 208 nm as a function of temperature. The values are reported as mean residue ellipticity. The abrupt upward jump at about 85°C in the signals is caused by the formation of insoluble aggregates. (**d**) Thermal denaturation curves of HEK IgG 6B3 analogous to panel (c). The temperature of aggregation onset for this construct was found to be lowered to about 75°C. (**e**) Thermal denaturation curves of *Pichia*-produced IgG 2C2 variants. (**f**) Thermal denaturation curves of *Pichia*-produced IgG 6B3 variants.

domains, samples were further analyzed by ITF as a function of temperature. As ~70% of the tryptophan residues of the studied IgGs are localized in the Fab fragments, this method should be more sensitive to small changes in the stability of these parts of the molecule. As shown in Fig. 4a and b, the data derived from CD spectroscopy could be confirmed by ITF, validating the increased stability of the M variants. A clear difference in stabilities could be seen for the 6B3 constructs (Fig. 4b), where the IgG and Fab WT variants exhibited their transition at 67.6° ± 0.1°C and 69.7° ± 0.1°C and thus at lower temperatures compared with their engineered M counterparts with a transition at 70.8° ± 0.1°C and 74.2° ± 0.2°C, respectively. For the 2C2 constructs, the advantages of the M variants, however, were considerably less pronounced (Fig. 4a).

To probe whether differences in the temperature-induced unfolding of 2C2 might have been masked by intermolecular or intramolecular aggregation, the same IgG samples were analyzed in the presence of GdnHCl. After an overnight incubation in 1 M GdnHCl before being exposed to increasing temperature still in the presence of 1 M GdnHCl, both IgG variants were clearly destabilized and started to unfold at lower temperatures (Fig. 4c)—however, the M variant showed a slightly increased stability of the second transition at 71.8° ± 0.2°C, compared with its WT counterpart with 70.4° ± 0.3°C.

To finally challenge the stability of the engineered variant with yet another parameter, the thermal stabilities of the 6B3 WT and M molecules were determined over a broad pH range. As shown in Fig. 4d, the increased stability of the engineered IgG proved true in all tested buffer systems having pH values between 4 and 10. On average, the stabilities of the M variants were 3.3° ± 0.6°C higher than those of the corresponding WT molecules.

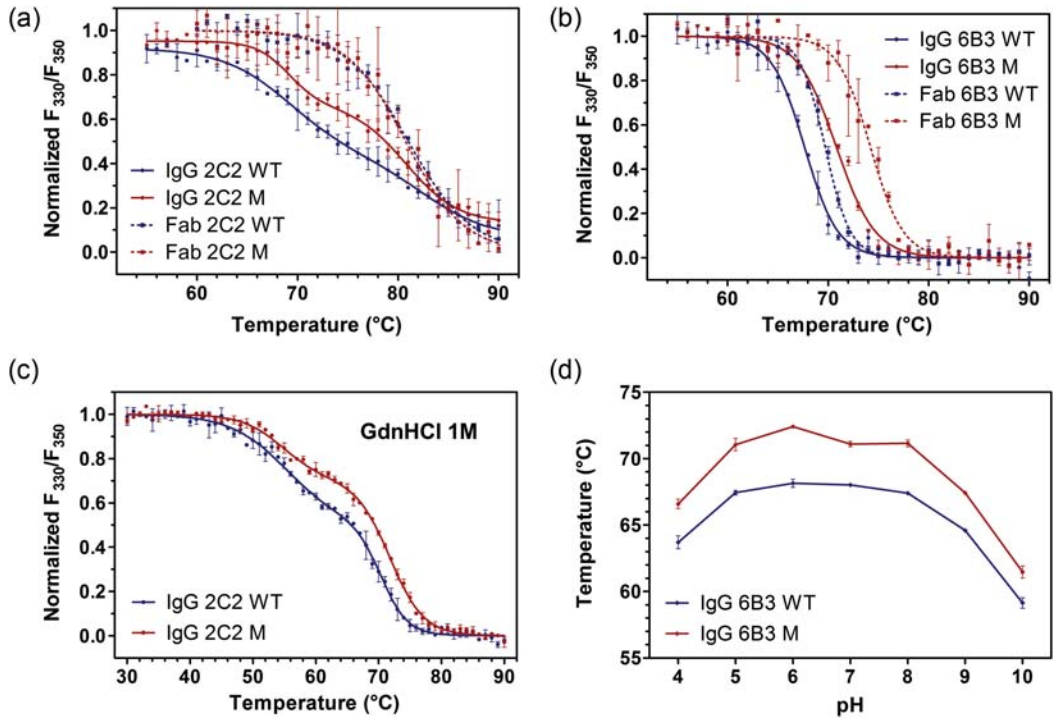

Fig. 4. Biophysical characterization of IgG and Fab constructs produced in mammalian cells by ITF. (**a**) Thermal denaturation curves measured by ITF. The curves were obtained from the intensity ratio of the emission spectrum at 330 nm (F_{330}) and 350 nm (F_{350}) upon excitation at 295 nm, plotted as a function of temperature. A comparison between the different mammalian IgG 2C2 (continuous lines) and Fab 2C2 (dotted lines) variants is shown. (**b**) Thermal denaturation curves of IgG 6B3 and Fab 6B3 measured analogously to the method used in panel (a). (**c**) ITF analysis of HEK IgG 2C2 in the presence of 1 M GdnHCl (**d**) pH dependence of thermal denaturation. The midpoints of the denaturation curves for HEK IgG 6B3 WT and M were determined at various pH and plotted as a function of pH.

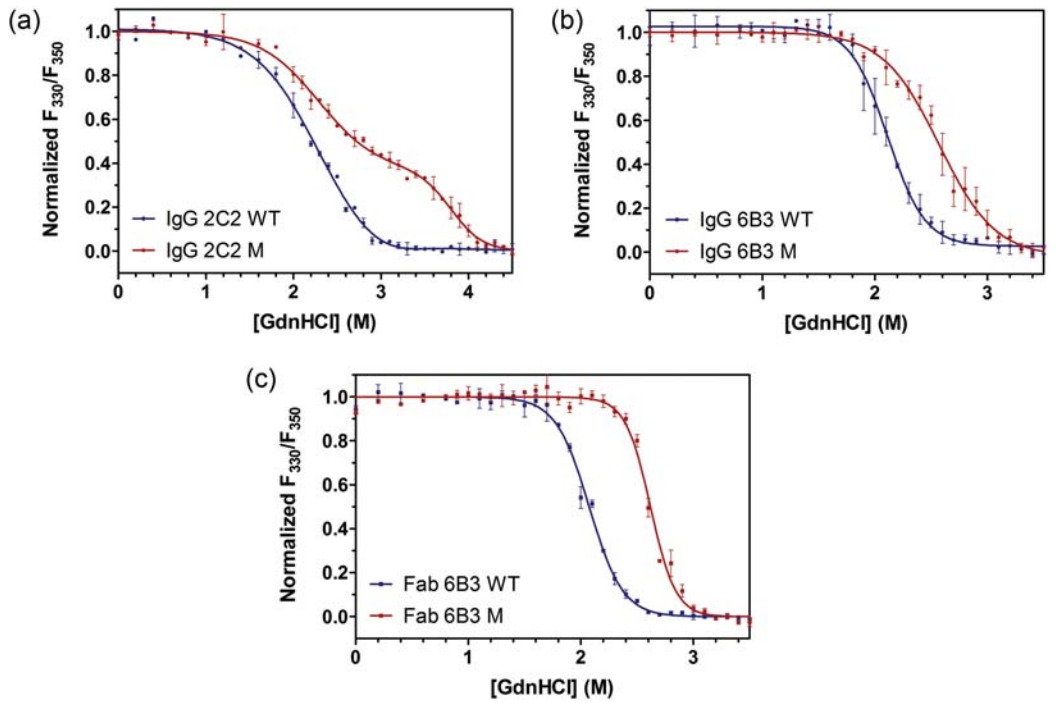

Fig. 5. GdnHCl-induced denaturation of IgGs expressed in mammalian cells. The denaturation of various antibody variants was followed by plotting the F_{330}/F_{350} ratio as a function of increasing GdnHCl concentration for (**a**) HEK IgG 2C2, (**b**) HEK IgG 6B3 and (**c**) HEK Fab 6B3.

The increased stability of the M variant over its WT counterpart was further investigated with respect to denaturant-induced unfolding. For this purpose, antibody molecules were incubated in various concentrations of GdnHCl and analyzed by ITF after an overnight incubation (Fig. 5). To better identify the signals derived from unfolding of the C_H2 domains, glycan knock-out T299A mutants were also examined (data not shown). Previous studies (Schaefer

and Plückthun, 2012) had clearly shown a decreased C_H2 stability for unglycosylated IgGs, and thus, the first transition e.g. at 2 M GdnHCl in Fig. 5a could be assigned to C_H2, as it shifted to even lower GdnHCl in the glycan knock-out mutant (data not shown). Thus, the second transition of the unfolding curves could be assigned to the Fab fragment.

For all analyzed antibody variants, the introduced mutations caused an increased stability compared with the respective WT. Whereas the transition due to the Fab fragment was detected in the WT variants of the 6B3 and 2C2 constructs at 2.0 and 2.5 M GdnHCl, the engineered mutants showed an increased Fab stability of 2.6 and 3.8 M, respectively. The same results were also obtained when the Fab 6B3 fragments were analyzed by themselves, i.e. as a produced Fab fragment (Fig. 5c). In addition to the differences in equilibrium stability, the kinetics of unfolding was considerably different between M and WT for some conditions and thus amplified the stability differences, as illustrated in time-dependent unfolding studies displayed in Supplementary Data Fig. S4. Although resulting in the same signal after an overnight incubation, the presence of, e.g. 4.5 M GdnHCl was sufficient to denature the 2C2 WT variant completely within ~10 min while IgG 2C2 M was not fully unfolded in the same GdnHCl concentration even after 2 h. Analogous results were obtained for the 6B3 constructs in the presence of, e.g. 3.5 M of denaturant.

Analysis of the antibody molecules on the domain level

Finally, we aimed to investigate the effect of the V_H mutations within the antibody at the level of individual domains or interacting folding units. The methods of choice for these studies are DSC or DSF. DSF has the advantage of small sample requirements and easy sample preparation, making it suitable for high-throughput applications and initial screens. However, the nature of transitions is much more difficult to assign, and changes in later transitions (i.e. more stable domains) are more difficult to detect. For IgGs, the transition of the C_H2 unfolding detected at 72°C emerged to be the

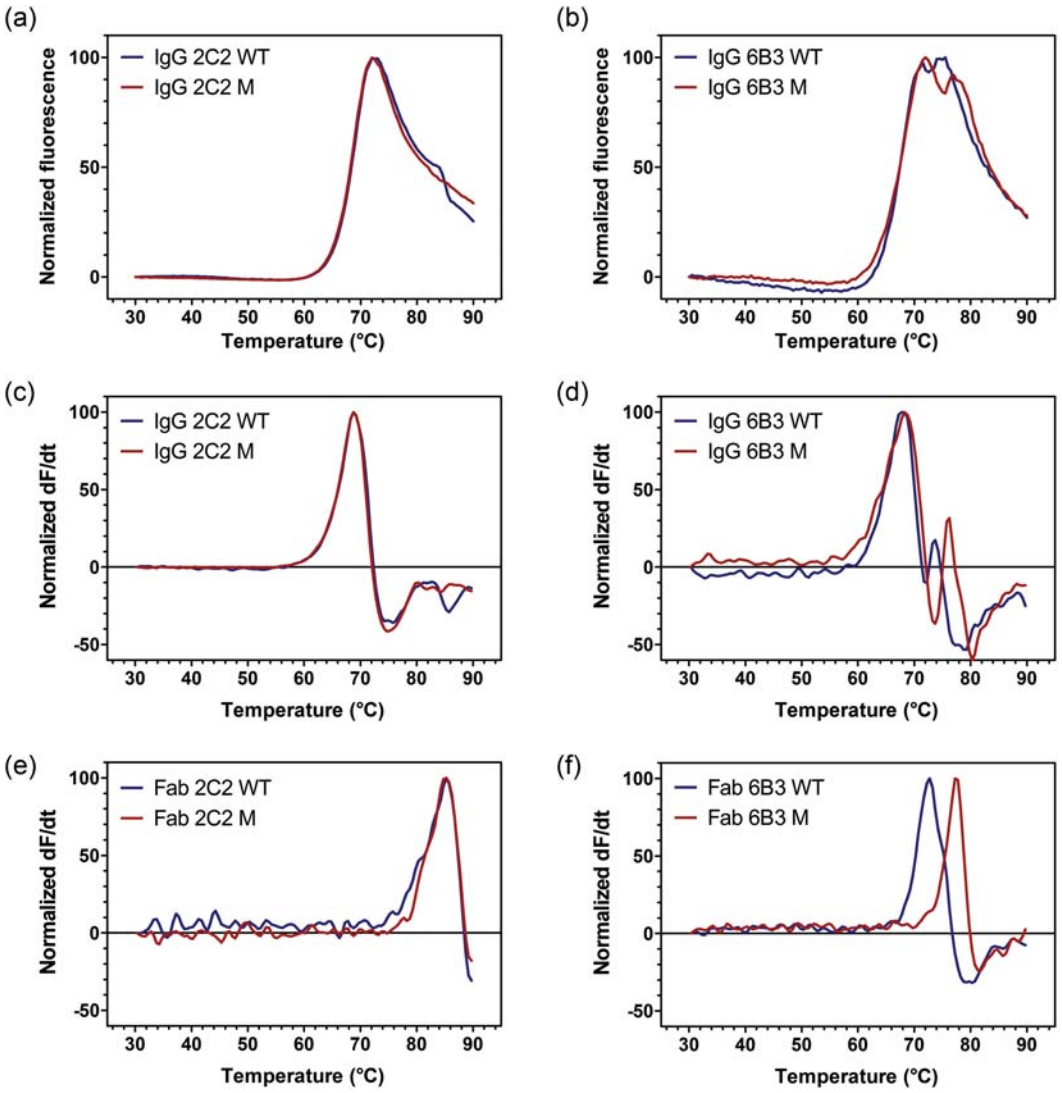

Fig. 6. Characterization of HEK-produced antibodies by DSF. Comparison of normalized DSF signals of HEK-produced antibody WT (blue) and M (red) variants. For the IgGs, the transition of the C_H2 unfolding is the dominant signal detected. DSF spectra were recorded for (**a**) IgG 2C2 and (**b**) IgG 6B3. For an easier comparison, the corresponding normalized first derivatives (d*F*/d*t*) of the signals in (a) and (b) are shown in (**c**) for IgG 2C2 and in (**d**) for IgG 6B3. The d*F*/d*t* graphs for the corresponding Fab-fragments are depicted in (**e**) for Fab 2C2 and in (**f**) for Fab 6B3.

most dominant signal, making the detection of later transitions involving the most relevant part of the molecule, the Fab fragment, quite difficult or even impossible (Fig. 6).

Although the transition of a second domain could still be clearly seen for the 6B3 construct (74.5°C vs. 77°C for WT and M variants, respectively, as depicted in Fig. 6b), DSF showed apparent limitations in the analysis of Fab fragments with very high stabilities. In the 2C2 variants only slight differences were detectable at ~84°C in Fig. 6a. For comparison, also the corresponding first derivatives (d*F*/d*t*) were plotted in Fig. 6c and d, highlighting again the differences in the second domain transition for the 6B3 IgGs (73.8°C vs. 76.3°C). These signals could be definitely attributed to the corresponding Fab domains, as they matched the data obtained from the corresponding recombinant Fab fragments (Fig. 6e and f). For the 6B3 Fab variants, the transitions were determined to be 72.8°C or 77.3°C and thus 4.5°C apart.

As DSF proved to be limited in its analytical potential of domains with much higher stabilities than the first transition, antibody samples were also subjected to DSC analysis (Fig. 7). These analyses require more time and sample, but can resolve three major transitions originating from the C_H2, C_H3 and Fab fragments, as is typically seen for IgG (Garber and Demarest, 2007). Yet for most of our samples, some of these peaks were overlapping. However, combining the results from both 2C2 and 6B3 constructs as well as from the T299A glycan knock-out mutants with their lowered C_H2 stability (Fig. 7e), clear assignments could be made. Whereas the transitions of the glycosylated C_H2 and of the C_H3 domains were detected at 70.1°C or 81.3°C, respectively, the signals of the different WT and M Fab fragments were found between 70°C and 88°C for the 6B3 and 2C2 construct.

In agreement with the results from the other analysis techniques detailed above, the Fab fragment of the engineered 6B3 M variant was of higher stability than its WT counterpart (on average 2.5°C). This could be detected for the IgGs produced in HEK (Fig. 7b), in *Pichia* (Fig. 7d) as well as for the HEK-produced Fab fragments (Fig. 7f). Interestingly, for

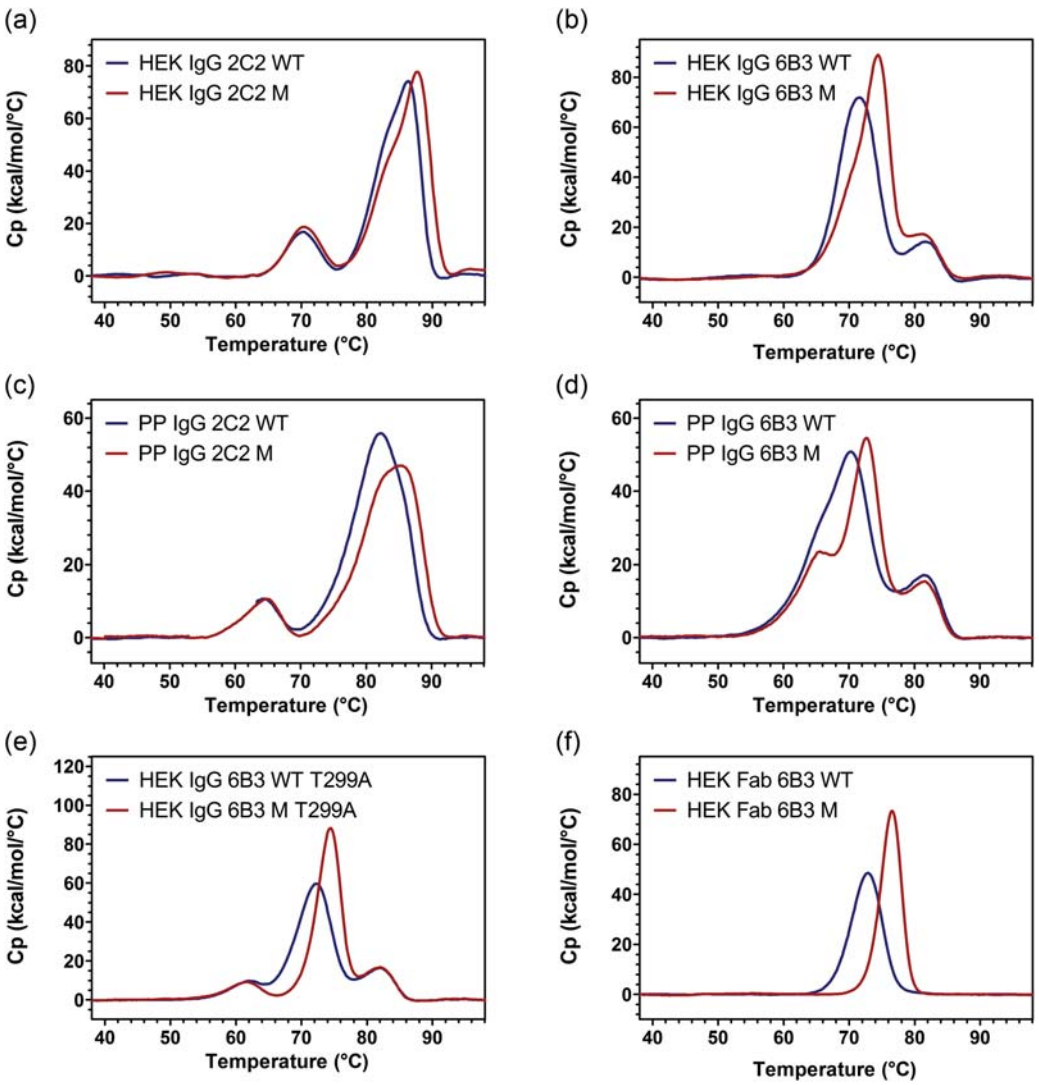

Fig. 7. Analysis of IgG domain stability by DSC. Signals derived from WT variants are shown in blue while those of the mutant M are represented in red. DSC curves were recorded for (**a**) HEK IgG 2C2, (**b**) HEK IgG 6B3, (**c**) PP IgG 2C2, (**d**) PP IgG 6B3, (**e**) HEK IgG 6B3 T299A and (**f**) HEK Fab 6B3.

the first time also small differences in the thermodynamic stability could be demonstrated for the 2C2 Fab construct (Fig. 7a and c). The signals of the mutated Fab fragments showed a melting temperature which was ~1.8°C higher than that of the WT variants and this difference was found for IgGs expressed in either the HEK or *Pichia* system, respectively. A comparison of the DSF and DSC derived data is presented in Supplementary Data Fig. S5.

Electrophoretic analyses of various IgG variants

When full-length IgGs were run on a gradient gel under non-reducing conditions and without prior heating (Fig. 8a), clear differences for the WT and M variants were encountered. Independent of whether the IgGs had been purified from HEK or *Pichia* cultures, WT IgGs usually could not be detected as a clear band at the corresponding size of 150 kDa, but rather as a smear or overlay of several individual bands. In contrast, the M variant gave rise to one clear and distinct band on Coomassie-stained gels (especially the 6B3 constructs, shown on the right side of the gel in Fig. 8a). To investigate this peculiar difference in running behavior between WT and M versions of the IgGs in more detail and at greater resolution, the same samples were run under identical conditions on low-percentage (7.5%) SDS polyacrylamide gels (Fig. 8b). Again, the engineered mutants could be detected as one distinct band, while for the WT variant several bands became visible. Interestingly, all these WT bands ran at slightly higher apparent molecular weights than the M counterparts—a feature that could be observed independent of whether the IgGs have been purified from stable HEK or *Pichia* cells.

To ensure that these differences between WT and M were not caused by effects of protein purification or storage, we also analyzed the non-processed supernatants of Chinese hamster ovary cells after transient transfection (CHO_t) and compared it to that of HEK293 cells after transient (HEK_t) or stable (HEK_s) transfection, respectively. As can be seen in Fig. 8c, the same banding patterns were observed in all cases and further confirmed for the yeast system as well (data not shown). To ensure that the differences in the running behavior were not caused by variations in the glycan moiety attached to the C_H2 domain of the IgG, antibodies with the glycan knock-out T299A mutation were also analyzed by SDS-PAGE. Whereas as expected, the unglycosylated IgGs ran generally at slightly lower apparent molecular weights, the banding pattern was not altered (Fig. 8d).

To test for covalent heterogeneities, we subsequently performed IEF analyses. In this method, the samples were

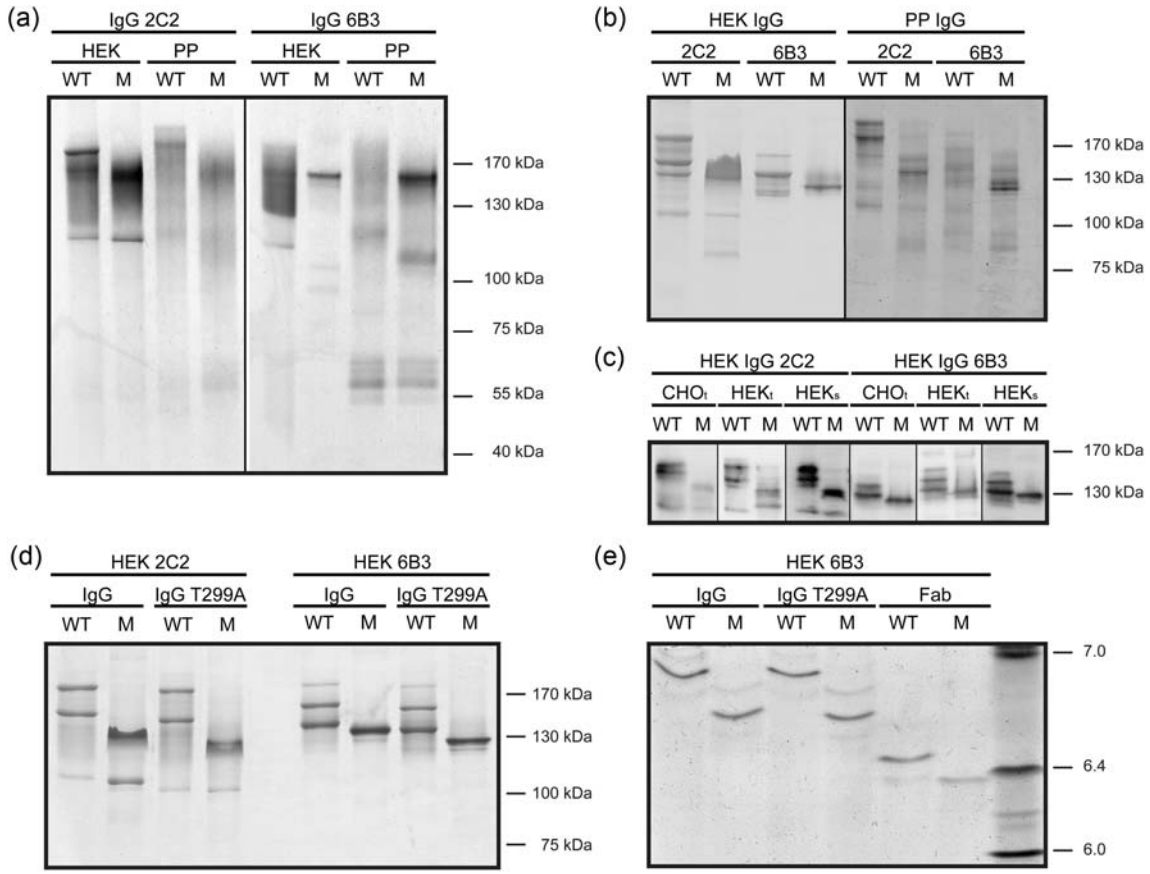

Fig. 8. Analysis of running behavior of IgGs on SDS-PAGE and IEF. (**a**) SDS-PAGE of equal amounts of the Protein A-purified HEK and *Pichia* constructs stained with Coomassie Blue. Samples were run under non-reducing conditions without heating prior to loading onto NuPAGE gradient gels. (**b**) SDS-PAGE analysis of the same samples as in panel (a) run on a low-percentage (7.5%) gel under the same, non-reducing conditions. (**c**) Western blot analysis of IgG variants detected with antibodies specific for the respective light chains. Samples were obtained from the supernatant of Chinese hamster ovary cells after transient transfection (CHO_t) and from HEK293 cells after transient (HEK_t) or stable (HEK_s) transfection, respectively. (**d**) Comparison of HEK IgG variants to their non-glycosylated counterparts (T299A glycan knock-outs) by non-reducing SDS-PAGE. (**e**) Isoelectric focusing of HEK-produced 6B3 variants. Non-reduced IgG, IgG T299A and Fab were separated based on their pI. A pI standard is shown in the right lane, with the corresponding pI values denoted next to it.

neither heated nor modified but just analyzed on pH gradient IEF gels. As the pIs of the 2C2 constructs were rather high (Fig. 1b), only the 6B3 constructs could be analyzed by IEF. As shown in Fig. 8e, all 6B3 constructs (IgG, IgG T299A as well as the Fab fragments) were focused in single major bands at positions of the gel corresponding to their pI, indicating that charge heterogeneity in the molecules was not the reason for the different running behavior on SDS-PAGE. The homogeneity of the samples was also confirmed by mass spectroscopy after prior reduction (data not shown), and is consistent with reducing SDS-PAGE (Fig. 1c) where no differences in the IgG chains between WT and M had been detected.

To further elucidate the reasons for the different running behaviors of the IgG variants, samples were once more studied by non-reducing SDS-PAGE (Fig. 9). This time, however, the samples were partly heated for 5 min at 95°C or alkylated prior to loading. Whereas the heating of the sample to 95°C eliminated the different running behavior of the variants (Fig. 9a), alkylation of samples by three different alkylation reagents did not change these characteristics (Fig. 9b).

We next considered the possibility that in the WT variants one or more disulfides might not have formed correctly and thus the molecules could have undergone disulfide shuffling, facilitated by sample heating. Previous studies showed that multiple bands for IgG samples on SDS-PAGE in principle can also arise from loss of disulfide-linked chains after disulfide scrambling (Liu *et al.*, 2007). Therefore, we wished to elucidate whether the different individual bands seen for the WT variants consisted of distinct covalent isoforms or whether all these bands were in equilibrium. For this reason, IgG 2C2 WT was run on a regular non-reducing 7.5% SDS-gel (after incubation in the absence or presence of alkylation reagent) and afterwards analyzed by a non-reducing second SDS-PAGE in a perpendicular orientation (see Fig. 9c and d and Materials and Methods for details). The silver-stained bands clearly indicated that the molecules found in each of the various individual bands in the first dimension differentiated again in the second dimension and gave rise to the usual banding pattern, independent of whether the samples had been alkylated beforehand or not. This finding would not be consistent with disulfide shuffling.

To test more rigorously whether the distinct bands of the WT are really in equilibrium, distinct bands of the WT and M variants were cut from the first gel and placed into the pockets of the second one (Fig. 9e). Again, the previously distinct bands re-divided into the original banding pattern. Due to the increased sensitivity of the silver staining procedure, even small amounts of the higher molecular weight bands could be detected for the M variant under these conditions. We thus can rule out disulfide shuffling as the source of the multiple bands detected for the WT IgG.

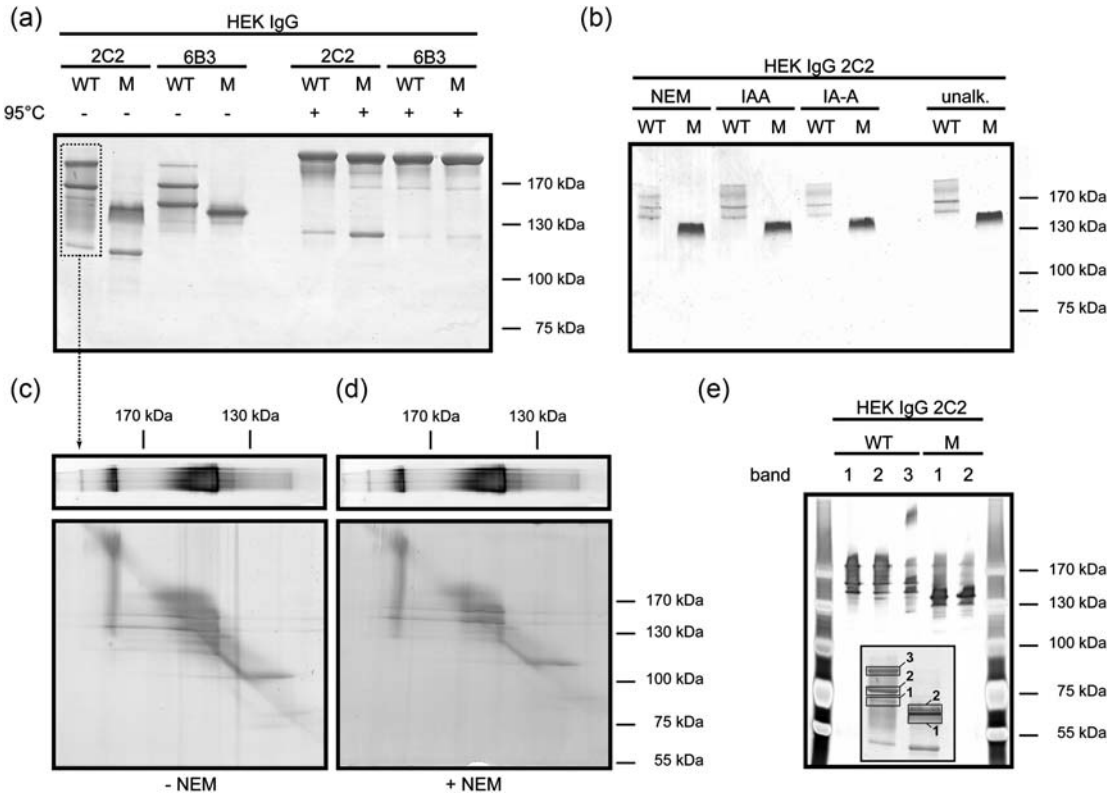

Fig. 9. One- and two-dimensional SDS-PAGE analysis of the different running behavior of WT and M variants. (**a**) Analysis of non-reduced IgG samples. Shown are the banding patterns of various IgG constructs after incubation in SDS-loading buffer at either room temperature or 95°C for 5 min prior to loading. (**b**) Influence of alkylation on banding patterns. IgG 2C2 samples were incubated with a 50-fold molar excess of *N*-ethylmaleimide (NEM), iodoacetamide (IAA) or iodoacetic acid (IA-A) in 100 mM Tris pH 8 (pH 7 for NEM) at 37°C for 3 h prior to analysis by non-reducing SDS-PAGE. (**c**) 2D-SDS-PAGE analysis of HEK IgG 2C2 WT. After the samples had been separated by regular non-reducing SDS-PAGE (shown on top, corresponding to the sample run on lane 1 of the gel depicted in panel (a)), the corresponding lane was isolated and re-run on a second SDS-PAGE in a perpendicular orientation. The final gel was silver-stained. (**d**) 2D-SDS-PAGE of the same sample as in panel (c). However, prior to the first SDS-PAGE, the sample was incubated in the presence of 5 mM NEM for 1 h. (**e**) 2D-SDS-PAGE of HEK IgG 2C2 WT and M. The bands were individually cut out from a first gel, as depicted in the inlay, and run in separate lanes on the second gel (corresponding to the band numbers in the first gel), and the gel was silver-stained.

Although both in this study and the one reported previously (Liu *et al.*, 2007) multiple bands of IgG have been seen under non-reducing conditions, there are important differences pointing to a different origin of the phenomena. Most importantly, in the experiments reported here the multiple bands *disappear* when the samples are heated to 95°C (Fig. 9a), while Liu *et al*. observed an *increase* of the banding pattern (i.e. more of the faster running bands) after prolonged heating and at high pH. Furthermore, in the re-equilibration experiments described above (Fig. 9c–e), all bands can be generated from all other bands (Fig. 9e), while Liu *et al*. observed an irreversible increase of smaller bands, consistent with a loss of chains from the H_2L_2 molecule. We therefore propose that the phenomena seen here are due to conformational rearrangements and *precede* any chain loss due to disulfide scrambling or progressive β-elimination (Liu *et al.*, 2007). This is consistent with the western blots, which indicate the presence of both chains in the high MW bands in Fig. 9, and the generation of a 100-kD band (representing H_2) only after prolonged mild reduction (see below). In summary, the conformational changes seen here are happening under much milder conditions than the chain loss described previously (Liu *et al.*, 2007) and represent conformational transitions of the intact IgG.

Capillary electrophoresis

To finally exclude that any particular effect of SDS-PAGE itself was causing the multiple band behavior, we also analyzed IgG samples by capillary electrophoresis. In this setup, the detection of the proteins was achieved using SDS micelles containing a provided fluorescent dye (Chen *et al.*, 2008). Upon binding to hydrophobic regions on the analyzed proteins, these SDS–dye complexes are protected from disassembly in the performed dilution step, generating a fluorescent signal clearly above background.

Also in this setup, multiple signals could be detected for the non-reduced, non-heated WT variants, as depicted for the IgG 6B3 WT in lane 1 in Fig. 10a and for IgG 2C2 WT in Fig. 10b. Strikingly, the M variants were not detectable at all under these conditions (lane 2 in Fig. 10a). Only once they had either been heated and/or reduced, equimolar amounts of the loaded M-type became visible in the corresponding chromatograms (Fig. 10c and d). Thus, the inability to detect the M variant under the initial conditions was not caused by too low IgG amounts loaded onto the chip, but rather hinted at a higher stability or improved folding of this molecule, preventing access to hydrophobic regions by the fluorescent dye used for detection in capillary electrophoresis. Thus, it did not bind to the native M protein, but only to the WT.

Partial reduction of IgG variants indicates differences in conformational stability

As these results indicated differences in the structural stability of the non-reduced, non-heated antibody molecules between their WT and M form, we analyzed HEK-produced IgGs by partial reduction. For this purpose, samples were

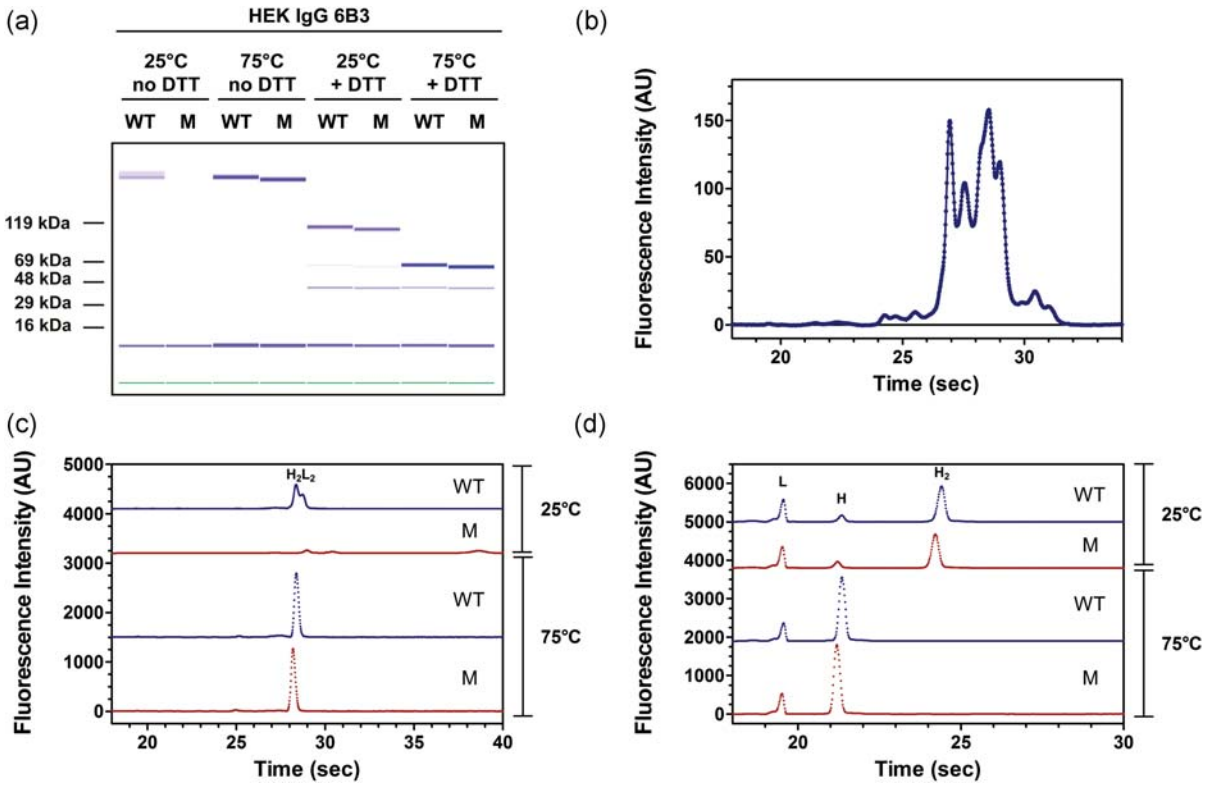

Fig. 10. Analysis of HEK IgGs by capillary electrophoresis. (**a**) HEK IgG 6B3 WT and M variants were analyzed in the absence or presence of reducing agent upon incubation in the loading buffer either at 25 or 75°C (presented as a virtual gel). The same data are presented as chromatograms in panels (c) and (d). (**b**) Chromatogram of HEK IgG 2C2 WT, illustrating the occurrence of similar differences in the banding pattern as detected by SDS-PAGE. (**c**) Chromatograms of IgG 6B3 samples analyzed under non-reducing conditions. H_2L_2 indicates the completely assembled IgG. (**d**) Chromatograms of the same samples as in (c), analyzed after incubation in the presence of DTT. H_2 indicates a heavy chain dimer and H or L the monomeric heavy or light chain molecules, respectively.

shortly incubated in the presence of the strongly reducing TCEP without any further heating prior to loading onto SDS-gels. We reasoned that the hydrophilic nature of TCEP should not allow it to easily penetrate into the hydrophobic cores of the IgG domains where the intradomain disulfides are located, without prior partial unfolding of the domains. Therefore, such partial reduction experiments represent an indicator for the compactness of these domains as well as the packing of the V_H-V_L interface.

As depicted in the Coomassie-stained gel and the corresponding anti-light chain western blot in Fig. 11a and b, respectively, incubation of the samples in the presence of TCEP seemed to disrupt the disulfide bond between the light and the heavy chain for both the 6B3 and the 2C2 constructs. Interestingly, a much more dramatic effect was observed for the WT constructs than for the M variants. Whereas IgG molecules containing a light chain could still be detected for both 6B3 constructs after TCEP reduction, all the HEK IgG 2C2 WT molecules were converted into homo-dimers of the heavy chain only (H_2 molecules running at ~100 kDa), completely lacking the light chains and therefore not being detectable in Fig. 11b, but only on the Coomassie-stained gel in Fig. 11a.

To confirm this observation, partly reduced 2C2 samples were treated with 5-IAF to fluorescently label free cysteine residues. Samples were incubated with very low TCEP concentrations, corresponding to only 2–10-fold molar equivalents, as higher concentrations were found to interfere with the subsequent 5-IAF coupling. Still, clear differences could be seen in the fluorescent images of non-reducing and reducing gels (Fig. 11c and d, top gels). Only the WT variant was labeled quantitatively at 2 molar equivalents and to a much higher extent at 10× conditions. Beneath the fluorescent images, the corresponding Coomassie-stained gels confirm that equal antibody amounts were loaded on the gels. Especially after overnight labeling with a 5-fold molar excess (Fig. 11e), the difference between WT and M variants became clearly visible, as the WT variant was labeled both on its heavy and light chain, while no fluorescence was detectable for the M counterpart.

Taken together, these data suggest that the introduced variable domain mutations, all located within V_H, affected the packing of the V_H-V_L and C_H1-C_L interface and thus protected the intermolecular disulfide bond. It is likely that this improved structural integrity potentially also contributed to the increased stability of the engineered M variants as a whole IgG molecule.

Discussion

The aim of this study was to analyze whether sequence engineering, previously found capable of considerably

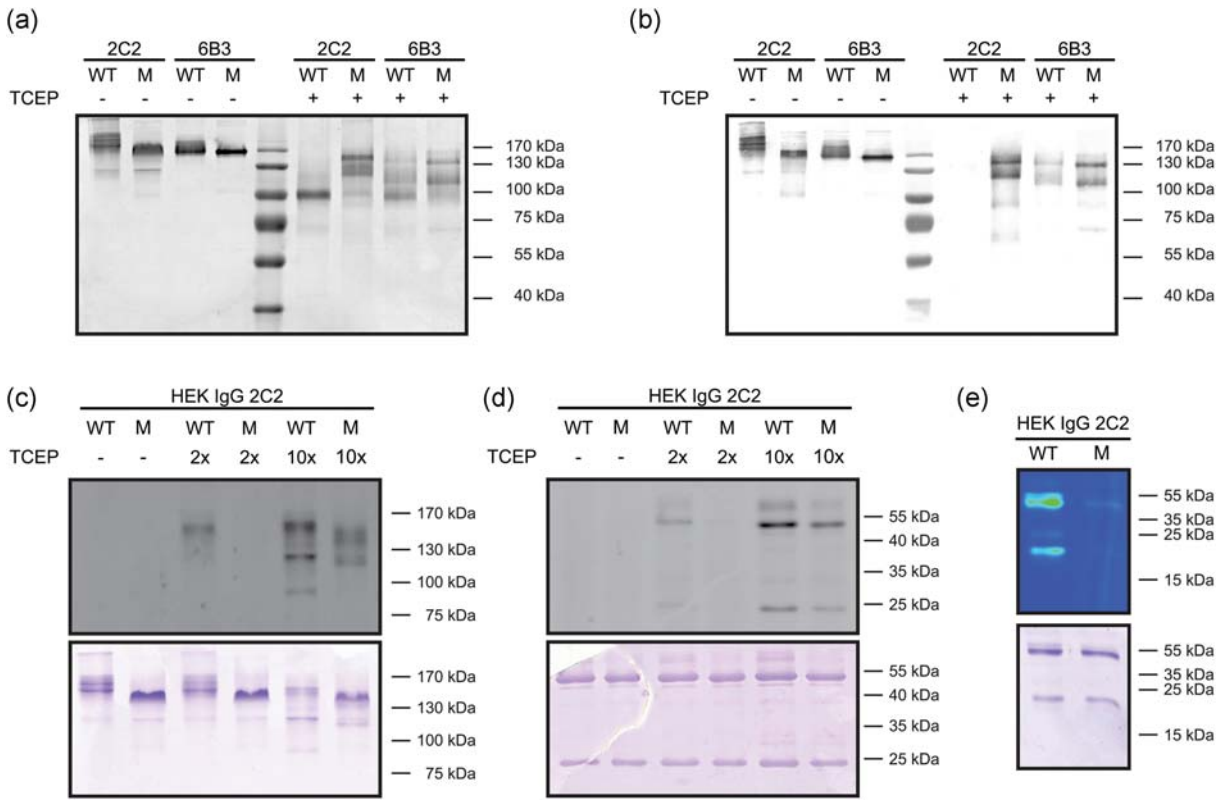

Fig. 11. Partial reduction of antibody variants. (**a**) Non-reducing SDS-PAGE of HEK constructs stained with Coomassie Blue. Samples were incubated in the absence or presence of 30 mM TCEP for 10 min at 25°C prior to loading. (**b**) Western blot analysis of the same samples as in panel (a) detected with an antibody mixture specific for both light chains. (**c**) Non-reducing SDS-PAGE of partially reduced HEK IgG 2C2 variants labeled with 5-IAF. Samples were incubated in the absence or presence of the stated molar equivalent of TCEP for 1 h at room temperature prior to labeling with a 5-fold molar excess of 5-IAF for 2 h. The upper gel shows the fluorescence image, the lower picture the same gel after staining with Coomassie Blue. (**d**) Images of the same samples as in (c) run under reducing conditions. (**e**) Comparison of WT and M variants reduced by 2 molar equivalents of TCEP for 1 h prior to labeling with a 5-fold molar excess of 5-IAF overnight. The upper gel shows the fluorescence image of a reducing gel, the lower one the Coomassie-stained gel.

improving the biophysical properties of antibodies as scFv fragments (Wörn and Plückthun, 2001), would have a similar effect on whole antibodies in the IgG format. The original work was carried out in single domains and smaller assemblies (Wörn and Plückthun, 1998, 2001; Ewert *et al.*, 2002; Ewert *et al.*, 2003a, Ewert *et al.*, 2003b; Monsellier and Bedouelle, 2006) as the extremely complex unfolding mechanism of IgGs (Buchner *et al.*, 1991; Vermeer and Norde, 2000; Feige *et al.*, 2010) with their 12 immunoglobulin domains interacting with each other would have made an elucidation of individual domain contributions and mutations impossible to untangle in the context of the whole antibody.

Despite the appeal of our previous reductionist approach, it was not clear *a priori*, whether the previous findings would be transferable from the scFv to the IgG format. It might be possible that the presence of the constant domains of the Fab fragment, especially when linked via an intermolecular C_H1-C_L disulfide bond (Röthlisberger *et al.*, 2005), overcomes stability problems within the variable domains themselves and/or at the V_H/V_L interface. Furthermore, the previous experiments were carried out with antibody fragments produced in functional form by secretion to the periplasm of *E. coli*. As whole IgGs are predominantly secreted from eukaryotic cells (although functional expression of IgG in *E. coli* has been reported as well; Simmons *et al.*, 2002; Mazor *et al.*, 2009; Makino *et al.*, 2011), it had to be investigated how the eukaryotic quality control system influences both the level and the properties of the resulting molecules, and whether it would be able to somehow compensate for the previously observed differences.

Thus, in this study we aimed to address these questions on two levels: first, the biophysical properties of the resulting proteins in isolation, and second, the influence of the expression systems used. To tackle these questions, we made use of an exceptionally well-characterized set of mutants (Ewert *et al.*, 2003a), where prior knowledge for each individual substitution (see Introduction) regarding their effect on thermodynamic stability or folding efficiency was available, measured by functional expression in *E. coli*. As an intermediate between scFv and IgG, we also constructed recombinant Fab fragments. To ensure meaningful results regarding the eukaryotic expression levels, we used homologous recombination into the same chromosomal location of the host cells as well as constitutive promoters for both the *Pichia* and HEK293 system.

Influence of the expression system

Unlike scFv produced in the bacterial periplasm, IgGs and Fab fragments expressed in both eukaryotic systems did not show any significant differences in their secretion yields found in the respective supernatants (Fig. 2). We also ensured that almost all of the antibody amounts synthesized by the cells were secreted (Supplementary Data Fig. S1a), excluding a bottleneck in secretion. Thus, these results derived from HEK and *Pichia* expression indicate that the eukaryotic secretory quality control system equalizes the expression yields of the WT and stabilized V_H6 variants, independent of the antibody format used. Interestingly, the leveling of expression yields is only partial in *Pichia* (with the stabilized mutants still producing slightly more antibody) but almost complete in the mammalian cells. Similar results had been previously obtained when engineered anti-tetanus toxoid Fab fragments were converted into the IgG format (Demarest *et al.*, 2006). Also for these Fab molecules the differences in the expression levels seen upon production in *E. coli* were not reflected in different levels of IgG found in mammalian expression.

We could show that the equalized expression levels are due to the eukaryotic host, and not the used IgG or Fab format. When comparing the periplasmic expression levels of full-length IgG in *E. coli*, we found the same increased expression levels for the engineered IgG molecules compared with WT as for the engineered scFv in *E. coli* (Supplementary Data Fig. S1b). However, as the expression levels of correctly assembled IgGs were generally low, no quantitative ELISAs could be performed, and these findings had to be obtained from western blot analysis.

Taken together, all these data indicate that stability engineering can improve bacterial expression and secretion of functional antibodies in all formats tested—single domain scFv, Fab, up to intact IgG—by mutations that prevent aggregation during periplasmic folding (Knappik and Plückthun, 1995; Nieba *et al.*, 1997; Ewert *et al.*, 2002, 2003a; Demarest *et al.*, 2006). However, the eukaryotic quality control can 'rescue' such aggregation-prone IgGs and secrete them at comparable level as the engineered mutants.

Analysis of biophysical properties of WT and M

To analyze whether the previously found improvements of the biophysical properties stayed true for various antibody formats produced in eukaryotic systems, sufficient quantities of the corresponding antibodies could be purified and analyzed (1–2 mg/l from *Pichia*, 4–8 mg/l from HEK293 cells), even though the constitutive expression systems were chosen for consistency, and not maximal yields.

Increased stabilities of the engineered IgGs (M variants) were observed by all analysis methods (Figs 3–7). The data derived from thermal denaturation measured by ITF, DSF and DSC as well as those from GdnHCl unfolding are summarized in Supplementary Data Table S1 for the HEK-produced IgG and Fab fragments. As the various methods emphasize different factors, the results listed are based on very different phenomena. Therefore, it is useful to briefly summarize what they actually indicate. In general, both CD and ITF measure averaged features of the whole antibody molecule—either the overall secondary structure or the averaged tryptophan fluorescence, respectively. In contrast, DSF and DSC have the ability, at least in principle, to distinguish different transitions in multidomain proteins (such as IgGs) which are averaged in the previously described spectroscopic methods.

The midpoints of thermal denaturation determined with CD and ITF were in quite good agreement with each other, with the ITF-recorded temperatures being of slightly lower values. Already at these lower temperatures, solvent may start penetrating into the protein core and may thereby make the environment of at least some tryptophans more hydrophilic, while the overall secondary structure measured by CD still is mainly intact. However, the increase in stability determined by both methods for HEK IgG 6B3 M over its WT counterpart gave very similar ΔT results of 2.5° or 3.2°C, respectively. These stability improvements were also in good agreement with the data recorded for the Fab fragments by DSF and DSC, even though the measured absolute transition

temperatures were of higher value, as the least stable C_H2 domain is not present in the Fab fragment und thus not taken into the average.

For IgGs, DSC analyses generally resulted in three distinguishable transitions, while in the DSF results often only the transition of the C_H2 unfolding could be clearly assigned (for comparison, see Supplementary Data Fig. S5). This finding can be explained by the fact that DSF measurements are based on intensity changes of the fluorescence of the dye SYPRO Orange as a function of its environment. Its fluorescence is weak in aqueous and hydrophilic environments, but strongly increases upon binding to hydrophobic patches that become accessible in denaturing proteins (Niesen *et al.*, 2007). After reaching a maximum, the signal decreases at higher temperatures. This is most likely caused by precipitation and aggregation of the analyzed protein, removing SYPRO Orange binding sites from solution. Therefore, the detection of high-temperature transitions, e.g. that of a very stable Fab within the IgG, is very challenging or even impossible.

In contrast, DSC measures the enthalpy of unfolding (Bruylants *et al.*, 2005) due to heat denaturation and thus allows the individual detection of various transitions. The DSC results clearly and directly confirmed the increased stabilities of the engineered IgG 2C2 and 6B3 molecules and could assign the effect, as expected, to the Fab fragment within the IgG.

Interestingly, the gain in thermal stability caused by the insertion of the six-point mutations was always higher in the context of the isolated Fab fragments compared with the gain recorded within the full-length IgGs. Not just the ITF data revealed a change of 4.5°C compared with only 3.2°C for the IgG molecule, but also the DSC data, allowing to clearly point to a Fab transition, showed an increase of 4°C for the stabilized isolated Fab fragment and 2.2°C for the Fab fragment in the context of the M IgG (Fig. 7f). At the moment, we have no definite explanation for this phenomenon, and want to stress that these data are derived from irreversible unfolding experiments, where the formation of aggregates could potentially affect the recorded data. We cannot exclude, however, that Fab unfolding might be influenced by interactions with the Fc part of the IgG, or that kinetic barriers are different for the Fab in isolation and within the IgG—a hypothesis that has been discussed controversially before (Kilar and Zavodszky, 1987; Lilie, 1997; Ionescu *et al.*, 2008).

Comparing the antibodies 2C2 and 6B3

The overall stabilities of the 2C2 and 6B3 constructs varied significantly, with the 2C2 construct in its WT state being already of quite high overall stability. Both antibodies differ in their light chains, with 2C2 containing a κ-light chain with $V_κ3$. This V_L domain had been shown previously (Ewert *et al.*, 2003b) to be of considerably higher stability when expressed individually than members of the $V_λ3$ family, which are present in the 6B3 construct. This difference in stability apparently stayed true in the context of single V_L domain, scFv, Fab and IgG, as shown in this study.

Thus, the two antibody constructs analyzed in this study covered a broad range of stabilities, from rather unstable (6B3 constructs) to extremely stable (2C2 constructs). This allowed us to show not only that our engineering strategy was successful in both cases, but also to evaluate analytical methods for detecting the effect in a stable and unstable IgG molecule. We found that most methods were unsuitable to characterize the stability gain of 2C2 M vs. 2C2 WT. Only for thermal denaturation measured by DSC as well as for GdnHCl-induced unfolding, improved stability characteristics of the 2C2 M molecules could be detected. For thermal unfolding studied by ITF, conclusive data could only be obtained in the presence of GdnHCl. For the 2C2 construct, however, the increase in stability was less pronounced with only ∼1.6°C compared with ∼2.5°C measured on average for the 6B3 constructs.

In GdnHCl-induced unfolding, the engineered variant of 6B3 denatured at a GdnHCl concentration 0.6 M higher than that of the WT counterpart, while this difference was ∼1.3 M for the 2C2 constructs. These data could also be confirmed by the analysis of the glycan knock-out T299A mutants (data not shown) and the individual Fab fragments. This difference in stability gain seems puzzling at first, as in thermal stability (measured by a variety of techniques) the impact of the mutations was more pronounced for the 6B3 constructs. However, we must consider two aspects, one regarding the measurements, the other regarding the denaturant: first, the unfolding of a multi-domain protein followed by ITF is very difficult to untangle in either temperature- or denaturant-induced unfolding, as the transitions are not separated and an intramolecular or intermolecular association of partially unfolded domains will influence tryptophan fluorescence. Second, GdnHCl may prevent such association of partially unfolded domains. Furthermore, the high ionic strength of concentrated GdnHCl may modulate electrostatic contributions during the unfolding. The two analyzed antibody constructs 2C2 and 6B3 possess rather different pI values and thus differ in their charge at any given pH. For these reasons, thermal unfolding may not necessarily be mirrored in GdnHCl unfolding (Monera *et al.*, 1994).

Although increased stabilities against thermal and denaturant-induced unfolding were also detected for M variants upon expression in *Pichia* (Fig. 3f or Fig. 7c and d), the melting points of IgGs produced in this system were generally lower than for the same IgG produced in mammalian cells. These different stabilities could be pinpointed to the C_H2 domains and proven to be caused by different glycan moieties, as described in detail elsewhere (Schaefer and Plückthun, 2012).

Inhomogeneity of WT but not M in SDS-PAGE

We noticed a consistent ladder formation of WT IgGs on non-reducing SDS-PAGE, whereas the mutants engineered for stability showed the expected unique band corresponding to a molecular weight of 150 kDa (Fig. 8a and b). Interestingly, also some commercially available antibodies like Omnitarg® (Pertuzumab, Genentech) showed similar banding patterns in our analyses (data not shown). Proteolysis could be ruled out as a cause considering the results from reducing SDS-PAGE (Fig. 1c). Similarly, heterogeneity of the glycan structure could be excluded by both IEF analysis (Fig. 8e) and the fact that the multiple band pattern was preserved in non-glycosylated T299A mutants (Fig. 8d).

We thus focused our attention on disulfide heterogeneities and/or scrambling, a problem reported to occur for some IgG4 molecules (Taylor *et al.*, 2006). Yet, alkylation of the

samples prior to loading did not affect the running behavior of the IgG (Fig. 9b). Thus, if different disulfide bond linkages were the reason for the detected phenotypes, they must have been already present in the purified samples. Such observations had been reported previously for a member of the IgG2 family (Wypych *et al.*, 2008). To test this possibility, we devised a non-conventional 2D-SDS-PAGE (Fig. 9c–e), in which non-reducing SDS-PAGE was carried out in both dimensions. In this setup, whole lanes or single bands were cut out and re-applied to a new gel. These experiments showed that the different bands could not be separated from each other but re-equilibrated in the second dimension, independent of whether the samples had been previously alkylated or not. We thus can conclude that the multiple bands are not due to disulfide heterogeneity.

This conclusion was further confirmed both by the analysis of unpaired cysteines within the IgG molecules as well as by mass spectrometry (MS) measurement. Quantification of free thiols by the method using sodium borohydride and 4,4′-dithiodipyridine described by Hansen *et al.* (2007) did not indicate any detectable free sulfhydryl groups for the WT and M variants (data not shown), even though this had been detected in other IgG molecules (Zhang and Czupryn, 2002). In addition, analyzing the disulfide patterns of enzymatically fragmented variants using liquid chromatography-mass spectrometry coupled to a combination of collision-induced dissociation and electron-transfer dissociation fragmentation (Wang *et al.*, 2011) did not provide any indications that wrong disulfide connectivities were present in any of the IgG variants (data not shown).

Stability probed by dye binding

Stabilized mutants and WT IgGs could be further distinguished by their accessibility either to a fluorescent dye from SDS micelles or to reducing agents. In capillary electrophoresis, which relies on detection of the proteins with SDS micelles containing a provided fluorescent dye (Chen *et al.*, 2008), the IgG WT, but not the M variant could be observed under non-reducing, non-heated conditions (Fig. 10). However, after heating and/or reduction both variants were equally well detected. These results could not be merely attributed to the very slightly increased hydrophobicity of the M variant, as it was increased only by one amino acid. Therefore, these results rather indicated that the engineered M-type IgGs are more densely packed and, consequently, less label-containing SDS micelles can bind to or penetrate into their structure.

These capillary electrophoresis experiments have some similarity to DSF analyses. However, whereas in DSF experiment the IgG is heated and the binding of the SYPRO Orange dye is followed as a function of temperature, capillary electrophoresis is isothermal and thus can be carried out below the denaturation temperature. At this temperature, SDS seems to allow access of the dye only to the WT, but not to the stabilized mutant. This is remarkable, as the DSC experiments showed that the C_H2 domains denatured first, and these domains are identical for WT and M. Thus, the significant differences detected for M and WT variants in the capillary electrophoresis experiment must be due to the dye's accessibility to binding sites within the Fab fragment.

Stability probed by partial reduction

Intermediates in the denaturation and reduction of IgGs have been monitored before, both by SDS-PAGE and by capillary electrophoresis (Alexander and Hughes, 1995; Brody, 1997). However, we believe that this study is the first to compare point mutants in the IgG format using these techniques. In partial reduction experiments with TCEP, clear differences in the accessibility of the inter-chain H–L disulfide bond could be detected. The WT variants, but not their M counterparts were losing their light chains (which were identical in both mutants) either to a large extent or completely, as confirmed by both western blot analysis and fluorescent labeling of the liberated thiol groups. This finding was rather astonishing, as all introduced mutations are located within the V_H domain, while the disulfide bond connects the distal ends of C_H1 and C_L. Thus, these data suggest a weakening of the H/L interface which is felt throughout the whole Fab fragment.

Taken together, these results support our assumption that the performed mutations do not just influence the stability of the resulting IgGs in the domain where the mutations are localized (V_H), but also a domain distal to it thus affecting the overall integrity and structural homogeneity of the IgG molecules. It is well established that IgG domains other than the C_H2 (due to its glycosylation) interact strongly in a lateral fashion, forming $V_H–V_L$, $C_L–C_H1$ and $C_H3–C_H3$ modules, respectively (Röthlisberger *et al.*, 2005). In contrast to these strong lateral interactions, longitudinal interactions generally are reported to be rather weak or even nonexistent. Nevertheless, the ball and socket joints between the V_H and C_H1 or V_L and C_L domains, respectively, combined with some movement within the $V_H–V_L$ interface provide some structural variation to the Fab fragment (Lesk and Chothia, 1988) that could partially explain the detected results.

Whether, however, structural changes within the Fab fragment can be transmitted to the constant domains within the Fc part has been controversially discussed for a long time (Simon and Rajewsky, 1990; Pritsch *et al.*, 1996; Morrison *et al.*, 1998; Chan *et al.*, 2004; Röthlisberger *et al.*, 2005). Our results do not indicate such interactions in the native molecule, and the observations may be explained without postulating them. Mutations within the V_H domain could affect the $V_H–V_L$ interface, which by the coupling within the Fab fragment (Röthlisberger *et al.*, 2005) could lead to the observed facilitated reduction of the $C_H1–C_L$ disulfide. Antibodies having lost their light chains may subsequently show a different susceptibility to reducing agents in the hinge region and other domains in the Fc part. As a corollary, we can consider the variable domains as a potentially weak link, and the engineering of this domain can make a decisive improvement in stability—even for the whole IgG molecule, as shown by this study.

Conclusions

Taken together, the present data clearly indicate that the mutations introduced into the V_H6 framework have beneficial effects not just in the scFv context but also in the IgG format. Although an increase in expression levels was only detectable for periplasmic expression in *E. coli*, increased stabilities both with respect to thermal and denaturant-induced unfolding of both Fab fragments and full-length IgG were seen,

independently of the expression host. These mutations proved to be beneficial independent of the nature of the light chain and could be applied to IgGs of rather distinct characteristics concerning their pI values and Fab stabilities. The mutations also influenced the structural integrity and homogeneity of the engineered IgG molecules independently of any wrong disulfide bond connectivity. Presumably through an improved V_H–V_L packing, the reduction of the intermolecular C_H1–C_L disulfide was greatly slowed down in the stabilized variant. These results confirm the potential of structure-based protein engineering in the context of full-length IgGs and the transferability of improvements discovered in a systematic study of smaller antibody fragments. Furthermore, it refocusses the engineering of intact antibodies to the variable regions, while in recent years it has mostly been concentrated on the constant Fc part.

Supplementary data

Supplementary data are available at *PEDS* online.

Acknowledgements

The authors thank Dr P. Gimeson (GE Healthcare, Sweden), Dr T. Müller-Späth (ChromaCon, Switzerland) and Dr D. Weinfurtner (MorphoSys, Germany) for their help with the DSC, CIEX and Capillary electrophoresis experiments, respectively. They acknowledge Dr M. Heller (University of Bern, Switzerland) for his MS analyses and active help in their interpretation. The authors are further grateful to the personnel of the Functional Genomics Center at University of Zurich for their help with MS analyses and RP-HPLC. The authors' thanks are also due to Dr S. Duhr (NanoTemper, Germany) for his help in determining affinities by microscale thermophoresis. They further thank Dr P. Lindner for critically reading the manuscript and for valuable suggestions, and the other members of the Plückthun laboratory for fruitful discussions.

Funding

J.S. was recipient of a Kekulé predoctoral fellowship of the German Chemical Industry Association and a member of the Molecular Life Science Ph.D. program. This work was supported by the Schweizerische Nationalfonds (SNF) grant 3100A0-128671/1 (to A.P.).

References

Alexander,A.J. and Hughes,D.E. (1995) *Anal. Chem.*, **67**, 3626–3632.
An,Z. (2010) *Protein Cell*, **1**, 319–330.
Anelli,T. and Sitia,R. (2008) *EMBO J.*, **27**, 315–327.
Bass,S., Gu,Q. and Christen,A. (1996) *J. Bacteriol.*, **178**, 1154–1161.
Beck,A., Wurch,T., Bailly,C. and Corvaia,N. (2010) *Nat. Rev. Immunol.*, **10**, 345–352.
Brandts,J.F., Hu,C.Q., Lin,L.N. and Mos,M.T. (1989) *Biochemistry*, **28**, 8588–8596.
Brody,T. (1997) *Anal. Biochem.*, **247**, 247–256.
Bruylants,G., Wouters,J. and Michaux,C. (2005) *Curr. Med. Chem.*, **12**, 2011–2020.
Buchner,J., Renner,M., Lilie,H., Hinz,H.J., Jaenicke,R., Kiefhaber,T. and Rudolph,R. (1991) *Biochemistry*, **30**, 6922–6929.
Cesaro-Tadic,S., Lagos,D., Honegger,A., Rickard,J.H., Partridge,L.J., Blackburn,G.M. and Plückthun,A. (2003) *Nat. Biotechnol.*, **21**, 679–685.
Chan,L.A., Phillips,M.L., Wims,L.A., Trinh,K.R., Denham,J. and Morrison,S.L. (2004) *Mol. Immunol.*, **41**, 527–538.
Chen,X., Tang,K., Lee,M. and Flynn,G.C. (2008) *Electrophoresis*, **29**, 4993–5002.
Cregg,J.M., Tolstorukov,I., Kusari,A., Sunga,J., Madden,K. and Chappell,T. (2009) *Methods Enzymol.*, **463**, 169–189.
Demarest,S.J., Chen,G., Kimmel,B.E., *et al*. (2006) *Protein Eng. Des. Sel.*, **19**, 325–336.
Demarest,S.J. and Glaser,S.M. (2008) *Curr. Opin. Drug Discov. Devel.*, **11**, 675–687.
Dillon,T.M., Bondarenko,P.V., Rehder,D.S., Pipes,G.D., Kleemann,G.R. and Ricci,M.S. (2006) *J. Chromatogr. A*, **1120**, 112–120.
Dobson,C.M. (2003) *Nature*, **426**, 884–890.
Ewert,S., Cambillau,C., Conrath,K. and Plückthun,A. (2002) *Biochemistry*, **41**, 3628–3636.
Ewert,S., Honegger,A. and Plückthun,A. (2003a) *Biochemistry*, **42**, 1517–1528.
Ewert,S., Huber,T., Honegger,A. and Plückthun,A. (2003b) *J. Mol. Biol.*, **325**, 531–553.
Feige,M.J., Hendershot,L.M. and Buchner,J. (2010) *Trends Biochem. Sci.*, **35**, 189–198.
Garber,E. and Demarest,S.J. (2007) *Biochem. Biophys. Res. Commun.*, **355**, 751–757.
Ghetie,V. and Ward,E.S. (2000) *Annu. Rev. Immunol.*, **18**, 739–766.
Glockshuber,R., Malia,M., Pfitzinger,I. and Plückthun,A. (1990) *Biochemistry*, **29**, 1362–1367.
Hansen,R.E., Ostergaard,H., Norgaard,P. and Winther,J.R. (2007) *Anal. Biochem.*, **363**, 77–82.
Honegger,A. and Plückthun,A. (2001) *J. Mol. Biol.*, **309**, 657–670.
Huston,J.S., Levinson,D., Mudgett-Hunter,M., *et al*. (1988) *Proc. Natl. Acad. Sci. U S A*, **85**, 5879–5883.
Ionescu,R.M., Vlasak,J., Price,C. and Kirchmeier,M. (2008) *J. Pharm. Sci.*, **97**, 1414–1426.
Jefferis,R. (2009) *Trends Pharmacol. Sci.*, **30**, 356–362.
Jefferis,R., Lund,J. and Pound,J.D. (1998) *Immunol. Rev.*, **163**, 59–76.
Kaneko,E. and Niwa,R. (2011) *BioDrugs*, **25**, 1–11.
Kilar,F. and Zavodszky,P. (1987) *Eur. J. Biochem.*, **162**, 57–61.
Knappik,A., Ge,L., Honegger,A., *et al*. (2000) *J. Mol. Biol.*, **296**, 57–86.
Knappik,A. and Plückthun,A. (1995) *Protein Eng.*, **8**, 81–89.
Laemmli,U.K. (1970) *Nature*, **227**, 680–685.
Lazar,G.A., Dang,W., Karki,S., *et al*. (2006) *Proc. Natl. Acad. Sci. U S A*, **103**, 4005–4010.
Lesk,A.M. and Chothia,C. (1982) *J. Mol. Biol.*, **160**, 325–342.
Lesk,A.M. and Chothia,C. (1988) *Nature*, **335**, 188–190.
Lilie,H. (1997) *FEBS Lett.*, **417**, 239–242.
Liu,H., Gaza-Bulseco,G., Chumsae,C. and Newby-Kew,A. (2007) *Biotechnol. Lett.*, **29**, 1611–1622.
Lux,A. and Nimmerjahn,F. (2011) *Adv. Exp. Med. Biol.*, **780**, 113–124.
Maas,C., Hermeling,S., Bouma,B., Jiskoot,W. and Gebbink,M.F. (2007) *J. Biol. Chem.*, **282**, 2229–2236.
Makino,T., Skretas,G., Kang,T.H. and Georgiou,G. (2011) *Metab. Eng.*, **13**, 241–251.
Mazor,Y., Van Blarcom,T., Iverson,B.L. and Georgiou,G. (2009) *Methods Mol. Biol.*, **525**, 217–239, xiv.
Mian,I.S., Bradwell,A.R. and Olson,A.J. (1991) *J. Mol. Biol.*, **217**, 133–151.
Monera,O.D., Kay,C.M. and Hodges,R.S. (1994) *Protein Sci.*, **3**, 1984–1991.
Monsellier,E. and Bedouelle,H. (2006) *J. Mol. Biol.*, **362**, 580–593.
Morrison,S.L., Porter,S.B., Trinh,K.R., Wims,L.A., Denham,J. and Oi,V.T. (1998) *J. Immunol.*, **160**, 2802–2808.
Nieba,L., Honegger,A., Krebber,C. and Plückthun,A. (1997) *Protein Eng.*, **10**, 435–444.
Niesen,F.H., Berglund,H. and Vedadi,M. (2007) *Nat. Protoc.*, **2**, 2212–2221.
Padlan,E.A. (1994) *Mol. Immunol.*, **31**, 169–217.
Plückthun,A. and Moroney,S.E. (2005) In Knäblein,J. (ed.), *Modern Biopharmaceuticals*. Wiley-VCH, Weinheim, pp. 1147–1186.
Pritsch,O., Hudry-Clergeon,G., Buckle,M., Petillot,Y., Bouvet,J.P., Gagnon,J. and Dighiero,G. (1996) *J. Clin. Invest.*, **98**, 2235–2243.
Ricklin,D., Hajishengallis,G., Yang,K. and Lambris,J.D. (2010) *Nat. Immunol.*, **11**, 785–797.
Roopenian,D.C. and Akilesh,S. (2007) *Nat. Rev. Immunol.*, **7**, 715–725.
Röthlisberger,D., Honegger,A. and Plückthun,A. (2005) *J. Mol. Biol.*, **347**, 773–789.
Sambrook,J. and Russell,D.W. (2001) *Molecular Cloning: A Laboratory Manual*. 3rd edn, Cold Spring Harbor Laboratory Press, Cold Spring Harbor, NY.
Schaefer,J.V. and Plückthun,A. (2012) *J. Mol. Biol.*, **417**, 309–335.
Shields,R.L., Namenuk,A.K., Hong,K., *et al*. (2001) *J. Biol. Chem.*, **276**, 6591–6604.
Simmons,L.C., Reilly,D., Klimowski,L., *et al*. (2002) *J. Immunol. Methods*, **263**, 133–147.
Simon,T. and Rajewsky,K. (1990) *EMBO J.*, **9**, 1051–1056.
Singh,S.K., Afonina,N., Awwad,M., *et al*. (2010) *J. Pharm. Sci.*, **99**, 3302–3321.
Skerra,A. and Plückthun,A. (1988) *Science*, **240**, 1038–1041.

Strohl,W.R. (2009) *Curr. Opin. Biotechnol.*, **20**, 685–691.
Taylor,F.R., Prentice,H.L., Garber,E.A., Fajardo,H.A., Vasilyeva,E. and Blake Pepinsky,R. (2006) *Anal. Biochem.*, **353**, 204–208.
Vermeer,A.W. and Norde,W. (2000) *Biophys. J.*, **78**, 394–404.
Volkova,K.D., Kovalska,V.B. and Yarmoluk,S.M. (2007) *Biotech. Histochem.*, **82**, 201–208.
Wang,N., Smith,W.F., Miller,B.R., Aivazian,D., Lugovskoy,A.A., Reff,M.E., Glaser,S.M., Croner,L.J. and Demarest,S.J. (2009) *Proteins*, **76**, 99–114.
Wang,Y., Lu,Q., Wu,S.L., Karger,B.L. and Hancock,W.S. (2011) *Anal. Chem.*, **83**, 3133–3140.
Wienken,C.J., Baaske,P., Rothbauer,U., Braun,D. and Duhr,S. (2010) *Nat. Commun.*, **1**, 100.
Wörn,A. and Plückthun,A. (1998) *Biochemistry*, **37**, 13120–13127.
Wörn,A. and Plückthun,A. (1999) *Biochemistry*, **38**, 8739–8750.
Wörn,A. and Plückthun,A. (2001) *J. Mol. Biol.*, **305**, 989–1010.
Wypych,J., Li,M., Guo,A., *et al*. (2008) *J. Biol. Chem.*, **283**, 16194–16205.
Zhang,W. and Czupryn,M.J. (2002) *Biotechnol. Prog.*, **18**, 509–513.